UAB
Universitat Autònoma de Barcelona

Dipòsit digital de documents de la UAB

This is the **submitted version** of the journal article:

Dong, Xinping; Tariq, Akash; Graciano, Corina; [et al.]. «Afforestation-driven soil organic carbon stabilization in a hyper-arid desert : nonlinear dynamics and microbial drivers across a 22-year chronosequenc». Environmental Research, Vol. 282 (October 2025), art. 121989. DOI 10.1016/j.envres.2025.121989

This version is available at https://ddd.uab.cat/record/321786

under the terms of the IN COPYRIGHT license

Afforestation-driven soil organic carbon stabilization in a hyper-arid desert: nonlinear dynamics and microbial drivers across a 22-year chronosequence

Xinping Dong[a,b,c,d], Akash Tariq[a,b,c], Corina Graciano[e], Zhihao Zhang[a,b,c*], Yanju Gao[a,b,c], Maierdang Keyimu[a,b,c], Mengfei Cong[a,b,f], Guangxing Zhao[a,b,c,d], Jingming Yan[a,b,f], Weiqi Wang[g], Jordi Sardans[h,i], Josep Peñuelas[h,i], Fanjiang Zeng[a,b,c,d*]

[a]*Xinjiang Key Laboratory of Desert Plant Roots Ecology and Vegetation Restoration, Xinjiang Institute of Ecology and Geography, Chinese Academy of Sciences, Urumqi, 830011, China*

[b]*Cele National Station of Observation and Research for Desert-Grassland Ecosystems, Cele, 848300, China*

[c]*State Key Laboratory of Ecological Safety and Sustainable Development in Arid Land, Xinjiang Institute of Ecology and Geography, Chinese Academy of Sciences, Urumqi, 830011, China.*

[d]*University of Chinese Academy of Sciences, Beijing 100049, China*

[e]*Instituto de Fisiología Vegetal, Consejo Nacional de Investigaciones Científicas y Técnicas, Universidad Nacional de La Plata, 1900 La Plata, Provincia de Buenos Aires, Argentina*

[f]*College of Ecology and Environment, Xinjiang University, Urumqi 830046, China*

[g]*Institute of Geography, Fujian Normal University, Fuzhou 350007, China*

[h]*CSIC, Global Ecology Unit, CREAF-CSIC-UAB, Bellaterra, 08193 Barcelona, Catalonia, Spain*

[i]*CREAF, Cerdanyola del Vallès 08193, Catalonia, Spain*

[*]*Corresponding author at Xinjiang Key Laboratory of Desert Plant Roots Ecology and Vegetation Restoration, Xinjiang Institute of Ecology and Geography, Chinese Academy of Sciences, Urumqi, 830011, China. E-mail addresses: zhangzh@ms.xjb.ac.cn (Zhihao Zhang) fjzeng@ms.xjb.ac.cn (Fanjiang Zeng)*

Abstract

Desertification and soil carbon loss threaten arid ecosystem sustainability, yet the long-term stability of soil organic carbon (SOC) following afforestation in hyperarid regions remains poorly understood. Here, we investigated SOC dynamics across a 22-year *Populus alba* chronosequence at the Taklimakan Desert edge, combining physical fractionation (particulate- (POC) and mineral-associated organic carbon (MAOC) with microbial phospholipid fatty acid (PLFAs) and enzymatic analyses. Afforestation significantly increased SOC content by 50.97%–108.05%, with MAOC surging 100.94%–160.59% after 22 years (P<0.01). SOC stability (MAOC/POC ratio) peaked at 12 years before declining. Random forest modeling identified total nitrogen (TN) and available phosphorus (AP) as key drivers. Meanwhile, microbial metabolic limitations, assessing by the stoichiometric of soil extracellular enzymes, shifted from phosphorus limitation to carbon-phosphorus colimitation suppressed decomposition activity, enhancing SOC stability. This study provides the quantification of nonlinear SOC stability trajectories in hyperarid plantations, offering critical insights for optimizing afforestation age to enhance the stability of SOC. Our findings advance mechanistic understanding of SOC persistence in water-limited ecosystems and directly inform desertification control policies under climate change scenarios.

Keywords: Soil organic carbon fraction; Microbial metabolic limitations; Plantation; Taklimakan desert

1. Introduction

Arid and hyperarid regions, covering >14% of global terrestrial area, are expanding rapidly due to climate change and anthropogenic pressures, threatening ecosystem services and carbon (C) sequestration capacity (Tariq et al., 2024). Soil organic carbon (SOC) stability plays a pivotal role in mitigating land degradation and achieving carbon neutrality (Heckman et al., 2022; Li et al., 2023b). Afforestation, a cornerstone of global desertification control, has been widely implemented (Li et al., 2023c; Zhang et al., 2024a). The dynamics of SOC during afforestation are co-regulated by multiple factors, including stand ages, soil properties, plant-dive C input (quantity and quality), and microbial metabolic activity. However, its long-term effects on SOC dynamics in water-limited ecosystems remain contentious (Hong et al., 2020), impeding accurate estimates of soil C storage and balance.

SOC stability can be assessed by the proportion of stable C fractions (Yang et al., 2012). SOC was physically fractionated into coarse particulate organic C (cPOC), fine particulate organic C (fPOC), and mineral-associated organic C (MAOC) using a size-based separation method (Willard et al., 2024). The physical separation of SOC is a popular classical method, which is also the basis for understanding the response of SOC formation and persistence to environmental changes (Cotrufo et al., 2019; Witzgall et al., 2021). fPOC is generally derived from cPOC and acts as a transitional component before its incorporation into more stable C pools (Zhao et al., 2025a). Of those, cPOC and fPOC are less stable SOC fractions, composed mainly of structural polymers from partially decomposed plant residues (Willard et al., 2024). In contrast, microbial necromass and metabolites are the main C sources of MAOC, which are formed via "direct sorption pathway" with mineral particles or via the "in vivo microbial turnover pathway"(Liang et al., 2017), represents a more stable SOC fraction with a longer residence time (Sokol et al., 2019; Hansen et al., 2024). While short-term studies report SOC increases, decreases, or neutral responses to afforestation (Liu et al., 2018; Kong et al., 2022; Rohatyn et al., 2022), the lack of chronosequence data obscures stability patterns beyond decadal scales. SOC sequestration following afforestation largely depends on the magnitude of organic matter being stored in soil via these stabilization processes (Liu et al., 2020; Gu et al., 2024). Since cPOC, fPOC, and MAOC follow distinct formation and degradation pathways over time, SOC stability may respond differently to duration of the afforestation (Ghani et al., 2023). Determining the driving mechanism of SOC content and stability over stand ages is essential to optimize SOC pool management.

Existing frameworks emphasize plant C inputs or soil texture (Sokol et al., 2019; Hansen et al., 2024), but neglect interactions between microbial nutrient limitation and SOC fractions—

a critical gap given microbial mediation of MAOC formation. The conversion of natural ecosystems to plantations may lead to changes in SOC pools through multiple pathways, including altering plant-derived C inputs (Jackson et al., 2017; Ao et al., 2024), soil physicochemical properties (Liang et al., 2025), and microbial activities and decomposition processes (Su et al., 2023). Afforestation may promote the accumulation of POC and MAOC due to increased plant biomass inputs into the soil (Li et al., 2023c). However, these plant biomass inputs can also accelerate the decomposition of POC, potentially reducing its accumulation through a soil priming effect (Villarino et al., 2021). Furthermore, plant inputs may disrupt soil mineral-organic associations through rhizosphere processes, thereby promoting C loss from MAOC (Keiluweit et al., 2015; Kleber et al., 2015). Substantial evidence indicates that the stand ages significantly affect the composition of soil microbial communities (Li et al., 2023a; Cheng et al., 2024; Sacca et al., 2024), which may contribute differently to SOC degradation and MAOC formation (Zheng et al., 2022). These changes can disrupt the original formation and decomposition of SOC components (Yu et al., 2022). Microbes dynamically exhibit different resource limitations that trigger specific acquisition strategies (i.e., via their production of C, nitrogen (N), and phosphorus (P)-acquiring enzymes) to obtain C and nutrients from soil organic matter (SOM), which ultimately influences the C cycling dynamics (Phillips et al., 2013; Cheeke et al., 2017). It has been reported that the limitation of microbial N and P limitation exacerbate C limitation, which may, in turn, stimulate the decomposition of SOC by microbes (Cui et al., 2021), thereby providing additional C sources to meet microbial nutrient needs (Wang et al., 2020). Current models, largely derived from temperate or semiarid systems, fail to address extreme aridity constraints (e.g., high salinity, low clay content) that govern SOC stabilization in deserts (Zhang et al., 2024b). The mechanisms that govern SOC stability following afforestation in arid environments are likely to differ from those observed in other ecosystems.

Populus alba is a highly suitable species for combating land degradation in arid areas, attributable to its rapid growth, economic value, and resistance to drought and barren conditions (Ji et al., 2020; Xi et al., 2021; Wang et al., 2024a). Here, this study investigated SOC dynamics across a 22-year *P. alba* chronosequence at the Taklimakan Desert edge—the world's second-largest mobile desert. Integrating physical fractionation (Six et al., 2002b), microbial PLFAs profiling, and enzymatic stoichiometry, this study: (1) Quantify age-dependent shifts in SOC fractions (cPOC, fPOC, MAOC) and stability (MAOC/POC ratio) and (2) Decipher drivers linking soil properties, microbial metabolism, and SOC persistence. Our hypotheses were:1) afforestation would promote SOC content and its fractions, driven by plant biomass input, soil

nutrient availability, and microbial metabolic processes (including microbial community composition and nutrient limitation); (2) the stability of SOC would be improved due to a decrease in unstable C pools (e.g., plant-derived cPOC and fPOC) resulting from the introduction of external C sources. This study provides the empirical evidence of SOC content and stability trajectories in extreme deserts, offering actionable insights for optimizing afforestation strategies under escalating aridity.

2. Materials and methods

2.1 Site description and experimental design

The experiment was conducted at the Qira Oasis-Taklimakan Desert transition zone (37°01′N, 80°43′E), a hyperarid region with mean annual precipitation of 46.62 mm and evaporation of 2,700 mm (Gao et al., 2022b; Gao et al., 2024; Zhang et al., 2024b). A space-for-time substitution design was adopted, selecting *P. alba* plantations of 7-, 12-, and 22-year-old stands (7Y, 12Y, 22Y) and adjacent unreclaimed desert land (0Y) as control. The main vegetation of unreclaimed desert land was *Alhagi sparsifolia* Shap., *Karelinia caspia* (Pall.) Less., and *Populus euphratica* Oliv. Stand ages were verified via tree-ring cores using a Haglöf Increment Borer (Model 5.15 mm, Sweden) and cross-dating with local forestry records.

Four sampling plots (10 × 30 m) were established at each stand ages, and a total of 16 plots were established in our study. The forest plot and control plot spaced ≥1 km apart to minimize edge effects. All plots shared similar soil texture (Arenosols: 28.91% clay, 0.96% silt, 70.13% sand) and irrigation regime (flooding 2–3 times annually from July–September). Before soil sampling, plant height (PH) and diameter at breast height (DBH) were measured in April 2024 (active growth phase, Fig. 1 and Table S1). Four root and litter sampling points were randomly selected at each stand ages, and root cores were taken using a soil corer (5 cm in diameter) after removing the litter layer with the root auger positioned 20–30 cm from the base of the tree trunk. Root samples were taken from both the 0–30 cm and 30–60 cm soil depths for further analysis. Litter collectors with an area of 1 m^2 were randomly placed at each plot to collect litter. All root and litter samples were thoroughly cleaned and then dried to constant weight at 65°C, and then biomass ($g \cdot m^{-2}$) was calculated using an electronic balance (± 0.01g).

2.2 Soil sampling and processing

In April 2024 (active growth phase), after removing the litter layer, soil sampling was performed at 3 randomly selected points per plot. Those samples were collected using a soil

auger at depth intervals of 0–30 cm and 30–60 cm, with samples from the same horizon within each plot were thoroughly mixed and homogenized. In total, 32 representative samples (4 stand ages × 2 soil depths × 4 replicate plots) were obtained. All soil samples were sieved through a 2 mm mesh to remove debris, including stones and roots. Those soil was then divided into three portions: (i) one portion was temporarily stored at -4°C for measurement of soil ammonium nitrogen (NH_4^+-N), nitrate nitrogen (NO_3^--N), and extracellular enzyme activities; (ii) another was briefly stored at -80 °C to measure soil microbial phospholipid fatty acids (PLFAs); and (iii) the remaining portion was air-dried at room temperature for analyses of others soil properties.

2.3 Soil property analyses

The concentration of total nitrogen (TN) was determined with a Kjeldahl Nitrogen Analyzer (K1160, Jinan Hanon Instruments Co. Ltd., China) (Zhao et al., 2025b). Ammonium nitrogen (NH_4^+-N) and nitrate nitrogen (NO_3^--N) were determined by the spectrophotometry (Zhang et al., 2020). The levels of total phosphorus (TP) and total potassium (TK) were measured using inductively coupled plasma optical emission spectrometry (iCAP 6300, Thermo Elemental, USA) after the samples were digested in concentrated HNO_3 (Du et al., 2025). Available phosphorus (AP) was measured by sodium bicarbonate immersion-molybdenum antimony colorimetric method. Available potassium (AK) was determined by flame photometric method (Zhao et al., 2025b). The soil pH was measured with a soil-to-water ratio of 1:2.5 (w/v) using a pH meter (PHSJ-6L, INESA Scientific Instrument Co. Ltd., China)(Lin et al., 2024). The electrical conductivity (EC) was measured with a soil-to-water ratio of 1:5 (w/v) using an EC meter (DDSJ-319L, INESA Scientific Instrument Co. Ltd., China)(Gao et al., 2022a).

2.4 SOC fractionation

The SOC concentrations of bulk soil and fractions were measured using the $K_2Cr_2O_7$-H_2SO_4 oxidation method (Lettens et al., 2005). SOC was divided into cPOC, fPOC, and MAOC, as it is considered a more effective approach for investigating the dynamics of SOC. The methods for determining cPOC (250–2000 μm), fPOC (53–250 μm), and MAOC (53 μm) were based on the protocols outlined by predecessors (Hook and Burke et al., 2000; Six et al., 2002a). Briefly, 10 g of air-dried soil was dispersed in 30 mL of odium hexametaphosphate solution (5 % w/v) by shaking on a reciprocal shaker for 18 h (180 rpm). The dispersed sample was then passed through 250 μm and 53 μm sieves. The material retained on the 250 μm sieve was quantified as coarse particulate organic matter, while the fraction collected on the 53 μm sieve

was used to quantify fine particulate organic matter. The soil materials in the leachate that passed through the 53 μm sieve were finer mineral-associated fraction. The samples were dried at 50℃. Subsequently, the C concentration of each fraction sample was measured, and the C content of each fraction was calculated based on both the C concentration and the mass proportion of each fraction. The SOC stability index (SI) was calculated as (Zhao et al., 2025a):

$$Stability\ index(SI) = C_{recalcitrant} / C_{labile} \times 100\% = C_{MAOC} / (C_{cPOC} + C_{fPOC}) \times 100\% \quad (1)$$

where C_{MAOC}, C_{cPOC}, and C_{fPOC} are the MAOC concentration (g kg^{-1}), cPOC concentration (g kg^{-1}), and fPOC concentration (g kg^{-1}), respectively.

2.5 Microbial PLFA profiling and enzymatic activities

Phospholipid fatty acids (PLFAs), key components of living microbial cell membranes, serve as biomarkers for characterizing soil microbial community composition (Bossio and Scow et al., 1998). In short, approximately 8 g of fresh soil was extracted, fractionated, and purified. The 23 mL mixed solution of citric acid buffer, anhydrous methanol, and chloroform (v/v/v = 4/10/5) was added to the Teflon bottle, shaken for 2 h (oscillation frequency ≥ 250 rpm). Then total lipids were extracted by centrifugation for 10 min (25 ℃, 7,000 rpm). Subsequently, phospholipid fatty acids were isolated by silica gel column chromatography. After methyl esterification, the internal standard (C19:0) was added. After dissolving in n-hexane, it was determined by Thermo Fisher 1300 meteorological chromatograph (TRACE 1300). The amount of PLFAs in the sample was calculated according to the peak area of the internal standard PLFA 19:0. The area determined by GC-FID was used to calculate the abundance of PLFA markers and was expressed as nmol PLFAs per gram of dry soil. The representative markers of microbes (Total bacterial PLFAs, gram-positive bacteria (GP), gram-negative bacteria (GN), actinomycete bacteria, and fungal PLFAs groups) of specific PLFAs are shown in Table S1.

The activities of five soil enzymes related to soil C, N and P cycles were determined by microplate fluorescence assay. These enzymes included C-acquiring enzymes (BG: β-1,4-glucosidase; CBH: cellobiohydrolase), N-acquiring enzymes (NAG, β-1,4-N-acetylglucosaminidase; LAP; leucine aminopeptidase), and P-acquiring enzymes (ALP, alkaline phosphatase). A detailed description of these methods is provided in Supplementary Method S1.

This study used two common stoichiometric indications to estimate the microbial metabolic limitations. One way was to calculate enzymatic stoichiometric vector characteristics (including vector length and vector angle) (Moorhead et al., 2016). Vector length (equation (2))

indicates that a high vector length implies more microbial C limitation. A vector angle higher (equation (3)) than 45° represents the P limitation and conversely represents the N limitation. Another way was to use 1.0 as the perpendicular line along the axis of enzyme activity ratios (NAG+LAP)/AP as the x-axis and (BG+CBH)/(NAG+LAP) as the y-axis), four groups of microbial resource limitations (N limitation, P limitation, C and N colimitation and C and P colimitation) were categorized (Bai et al., 2021).

$$Vector\ length=\sqrt{(\ln(BG+CBH)/\ln(NAG+LAP))^2+(\ln(BG+CBH)/\ln AP)^2} \quad (2)$$

$$Vactor\ angle=\mathrm{DEGREES}\{\mathrm{ATAN2}[(\ln(BG+CBH)/\ln(AP)),(\ln(BG+CBH)/\ln(NAG+LAP))]\} \quad (3)$$

2.6 Statistical analyses

All statistical analyses were conducted using the R software (v4.2.1, R Core Team, 2022). Two-way analysis of variance (ANOVA) was employed to assess the impact of stand ages and soil depth on the soil properties, litter mass and root biomass, SOC fractions, PLFAs, and enzymatic activities. Before conducting the ANOVA, all the data underwent tests for normality and homogeneity of variance. Duncan's multiple range tests were performed to conduct multiple comparisons at statistical significance ($P < 0.05$). The t-test was used to compare the differences between the two soil layers. Pearson's correlation analysis was performed to examine the relationships between SOC fractions (cPOC, fPOC, MAOC) and plant inputs (litter mass and root biomass), soil physical and chemical properties (pH, EC, NH_4^+-N, NO_3^--N, AP, AK, TK, TP, TN), soil enzyme activity (ALP, LAP, CBH, NAG, BG), and soil microbial community (bacterial PLFAs, GN, GP, actinomycete, and fungal PLFAs). The random forest model, using the R "randomForest" package, was used to assess the effects of plant input, soil physical and chemical properties, soil enzyme activity, and soil microbial community on SOC fractions. The percentage increase in mean square error (%IncMSE) was used to evaluate the relative importance of these variables using "randomForest" and "rfPermute" packages (Ao et al., 2024). Partial least squares path modelling (PLS-PM) analysis was conducted using the "plspm" package in R.

3 Results

3.1 Litter mass, root biomass and soil properties

After afforestation, *P. alba* exhibited rapid growth, leading to increased plant litter and root biomass input (Fig. S1). Compared with uncultivated land (0Y), stand ages significantly increased the concentrations of soil TN, TK, AP, AK ($P < 0.01$, Table S3–S4). Conversely, pH, EC and NO_3^--N concentration decreased with stand ages ($P < 0.01$, Table S3–S4). The TN and

AP levels in topsoil were significantly higher than those in subsoil after afforestation ($P < 0.05$, Table S3–S4). The other properties showed no significant differences between the two soil depths. The interactions between stand ages and soil depth had a significantly effect on TP and TN ($P < 0.05$, Table S3–S4).

3.2 SOC *fractions and SOC stability*

Afforestation significantly increased SOC content across all stand ages (7Y, 12Y, 22Y) compared to unreclaimed desert soils (0Y). In topsoil (0–30 cm), SOC increased by 41.61% (7Y), 70.47% (12Y), and 108.05% (22Y), while subsoil (30–60 cm) showed smaller increments (23.87–52.26%) (Fig. 2a). SOC fractions exhibited distinct patterns. cPOC was increased by 138.76% in topsoil after 22Y but remained unchanged in subsoil (Fig. 2b). fPOC was rose by 69.05% (topsoil) and 30.00% (subsoil) at 22Y (Fig. 2c). MAOC was surged by 160.59% (topsoil) and 100.94% (subsoil) at 22Y, dominating SOC composition (Fig. 2d).

SOC stability (SI, MAOC/POC ratio) peaked at 12Y in both soil layers (Fig. 3), with MAOC contributing >60% to total SOC (Fig. S3). Beyond 12Y, MAOC proportion declined in topsoil, paralleled by rising cPOC and fPOC. Subsoil stability was lower than topsoil, but there was no significant difference, and they followed a similar trend.

3.3 Microbial community and enzymatic activity

Total bacterial and fungal phospholipid fatty acids (PLFAs) increased by 446.42–721.57% (bacteria), 305.89%–605.52% (GP), 375.82%–707.65% (GN), 1659.30%–4495.10% (actinomycete), and 569.99–1426.89% (fungi) post-afforestation (Fig. 4). Fungal dominance (F/B ratio) increased by 16.98-88.19% in topsoil correlated with SOC accumulation (Fig. 4).

C-acquiring enzymes (BG, CBH) and P-acquiring enzymes (ALP) rose significantly with stand ages (Fig. S4). Microbial metabolic constraints shifted from P limitation (0Y) to C-P colimitation (7Y–22Y), as indicated by vector analysis (Fig. 5).

3.4 Drivers of SOC content and stability

The correlation heatmap showed that SOC, SI, cPOC, fPOC and MAOC were significantly and positively correlated with TN, PLFAs, litter biomass, and root biomass (Fig. 6 and Fig. S5, $P < 0.05$). While they were significantly negatively correlated with pH and EC. Random forest analysis showed that environmental factors explained 91.51% ($P < 0.01$) of the variation in SOC content, and identified TN and AP as the primary predictors of SOC content (Fig.7a). PLS-PM revealed that soil physicochemical properties (e.g., reduced pH and EC) directly promoted

SOC accumulation (standardized effect = 0.794), while alleviated P limitation (vector angle < 45°) indirectly enhanced SOC stability (Fig. 7c-d).

4. Discussion

4.1 SOC content dynamics and its drivers

The literature suggested that the impact of afforestation on SOC was context-dependent: afforestation increased SOC in C-poor soil; whereas decreased in C-rich soil (Wang et al., 2024b). In tropical regions with C-rich soil, a meta-analysis showed that secondary forests stored less SOC than primary forests (−9%)(Don et al., 2011). However, in hyperarid regions with C-poor soil, afforestation with *P. alba* significantly increased SOC content by 42.37–73.38% compared to unreclaimed desert soils (Fig. 2a). This increase was more pronounced in topsoil (0–30 cm, with more roots), where SOC rose by 108.05% in 22-year-old stands, driven by elevated plant-derived inputs (litter and roots, Fig. S1) and improved soil nutrients (TN, AP; Tables S3–S4). These results align with global afforestation studies showing SOC accumulation in arid regions through enhanced biomass input and nutrient availability (Hong et al., 2020). However, the magnitude of increase here surpasses reports from semiarid plantations (Liu et al., 2018; Kong et al., 2022; Rohatyn et al., 2022), likely due to the extreme initial SOC depletion in desert soils.

Drivers of SOC content increase can be explained by following two reasons. Firstly, rapid *P. alba* growth amplified litter and root biomass (Fig. S1), directly supplying particulate organic C (cPOC, fPOC). This aligns with the "input-driven SOC accumulation" paradigm in barren ecosystems (Li et al., 2023c; Zhang et al., 2024a). Secondly, TN enrichment enhanced plant productivity (Frey et al., 2025), while AP facilitated mineral-organic complexation (Kaiser et al., 2004), jointly stabilizing MAOC (Fig. S6). Notably, fungal-dominated communities (increased F/B ratio; Fig. 4d) further promoted recalcitrant C processing, as fungi excel at decomposing lignin-rich litter (Pulleman et al., 2022).

4.2 SOC stability dynamics and its drivers

The SOC stability (MAOC/POC ratio) initially increased, peaking at 12 years, but declined thereafter (Fig. 3). MAOC dominated SOC fractions in mid-term stands (12Y), while cPOC and fPOC contributions rose in older stands (22Y), particularly in subsoil (Fig. S3). Unlike cropland-to-forest conversions where SOC stability decreases due to priming effects (Sharma et al., 2024), stability here improved with stand ages. This divergence underscores the unique

role of MAOC in low-clay desert soils, where saturation thresholds are delayed (Hassink et al., 1997; Begill et al., 2023). Another possible explanation for the change of SOC stability is the relationship between system C input and microbial activity (Li et al., 2023c; Tang et al., 2025). Post-afforestation, the input of plant biomass provides microorganisms with abundant nutrients and energy, leading a significant increase in the number of microorganisms (especially actinomycetes, Fig. 4). Actinomycetes (A-strategists) are efficient substrate users, investing more energy in metabolism, extracellular enzymes, or improving competitiveness than in growth (Tang et al., 2025). These metabolic processes will lead to a decrease in the stability of SOC.

Peak MAOC at 12 years (Fig. S3) likely reflects transient saturation of mineral-binding sites (Stewart et al., 2007; Cotrufo et al., 2019). Subsequent declines in older stands (22Y) may stem from root exudates disrupting mineral-organic associations (Keiluweit et al., 2015; Kleber et al., 2015), a process exacerbated in sandy soils with low clay content. Microbial P limitation was alleviated by AP accumulation (Fig. 5b), but rising microbial biomass (Fig. 4) intensified C competition, shifting limitations to C-P colimitation (Fig. 5d). Differently, in subtropical regions, citrus plantations alleviated soil microbial C limitation but aggravated N limitation, as microorganisms preference produce N-acquiring enzymes (Du et al., 2024). Furthermore, in barren desert ecosystems, limited C resources lead to increased competition between microbes and plants by soil nutrients, further aggravating the microbial C limitation. This view is also supported by a significant negative correlation between plant and microbial limitation (Ning et al., 2024). This constrained decomposition activity (Sinsabaugh and Shah et al., 2011; Mooshammer et al., 2014; Luo et al., 2019), indirectly stabilizing SOC.

4.3 Limitations and practical implications

In our study, we used a space-for-time substitution methodology, assuming that spatial and temporal variations are equivalent, which is a useful tool for management in various ecological systems (Boeraeve et al., 2018; Kreyling et al., 2025). However, there are several limitations/uncertainties in the space-for-time substitution approach. For example, the "space-for-time" substitution assumes environmental homogeneity across chronosequence plots, yet unmeasured variables (e.g., interannual precipitation shifts) may influence SOC dynamics. To mitigate this uncertainty in real-world afforestation projects, we recommend integrating long-term monitoring (e.g., decadal soil sampling) with climate-resilient tree species selection. For instance, prioritizing *P. alba* genotypes with deep-rooting traits could enhance SOC stability under fluctuating water availability.

Although soil microbial biomass accounts for only 2%–4% of SOC (Dalal et al., 1998),

its necromass continue to accumulate in the soil. In forest ecosystems, the contribution of microbial necromass C to SOC is 20%–80% (Chen et al., 2020; Wang et al., 2021). Thus, these earlier reports and the present findings indicate microbial necromass should also be considered while exploring the drivers of SOC stability. In addition, microbial C limitation was inferred indirectly via enzymatic stoichiometry, and mineral-organic interactions (e.g., Fe-SOC complexes) were not directly quantified. This gap highlights the need for adopting advanced techniques (e.g., ^{13}C-labeled root exudate tracing, XANES spectroscopy) in future afforestation trials to optimize organic-inorganic binding. Practically, soils with low clay content (e.g., desert Arenosols) may benefit from amendments like biochar or clay additions to enhance MAOC formation, though field trials are needed to validate efficacy.

Findings from this study are context-dependent, driven by hyperarid conditions (e.g., irrigation-induced salt leaching) (Della Maggiora et al., 2023). To broaden applicability, afforestation strategies should be tailored to local soil-climate contexts. In similar arid regions, seasonal flooding regimes (as used here) could be standardized to balance salt removal and SOC retention. Moreover, reduced irrigation frequency and intercropping with N-fixing species (e.g., *Alhagi sparsifolia*) may better synchronize C inputs with microbial demand, avoiding MAOC saturation-induced instability.

While *P. alba* afforestation enhanced SOC, large-scale monocultures risk biodiversity loss and water overconsumption in water-limited ecosystems (Liu et al., 2018; Kong et al., 2022; Rohatyn et al., 2022). Diversifying plantations with native drought-tolerant species (e.g., *Haloxylon ammodendron*) could balance C goals with ecological resilience. Additionally, coupling afforestation with grazing exclusion policies may prevent soil compaction, preserving SOC stability in fragile desert-oasis ecotones.

5. Conclusions

Afforestation with *P. alba* at the hyperarid desert edge significantly enhanced SOC content and stability, with stability peaking at 12 years before declining. Topsoil exhibited stronger SOC accumulation than subsoil, driven by synergistic effects of plant biomass inputs, soil nutrient enrichment (TN, AP), and fungal-dominated microbial processing. Microbial metabolic constraints shifted from P-limitation to C-P colimitation, indirectly stabilizing SOC by suppressing decomposition activity. This study underscores the potential of *P. alba* afforestation to enhance SOC pools in hyperarid deserts, while highlighting the need for adaptive management strategies to sustain long-term C stability amidst climatic and ecological uncertainties.

Acknowledgements

This work was financially supported by the Tianshan Talent Training Program (Grant No. 2023TSYCLJ0046), the Natural Science Foundation of Xinjiang Uygur Autonomous Region (Grant No. 2024D01A144), and Postdoctoral Fellowship Program of CPSF (Grant No. GZC20232964). Corina Graciano was funded by the Chinese Academy of Science (Grant No. PIFI 2021VBA0001). We would like to thank Zhang qingqing for field sampling. We would also like to Baihui Biotechnology Co. Ltd., Chengdu (www.baihuitech.cn) for PLFAs and enzymatic activities measurements. The authors are thankful to their colleagues for their help and support, and would like to thank all the reviewers who participated in the review.

Author Contributions

Xinping Dong: Conceptualization, Data curation, Visualization, Writing-original draft, Writing-review & editing; Zhihao Zhang: Formal analysis, Data curation, Visualization, Writing-review & editing. Mengfei Cong, Guangxing Zhao, Jingming Yan: Investigation, Methodology; Akash Tariq, Corina Graciano, Yanju Gao, Maierdang Keyimu, Weiqi Wang, Jordi Sardans, Josep Peñuelas: Formal analysis, Writing-review & editing, Validation, Software; Fanjiang Zeng: Funding acquisition, Methodology, Writing-review and editing, Supervision.

Data availability

Data will be made available upon request.

Statements and Declaration

The authors declare that they have no known competing financial interests or personal relationships that could have appeared to influence the work reported in this paper.

References

Ao, D., Wang B., Wang Y., Chen Y., Anum R., Feng C., Ji M., Liang C., An S. 2024. Grassland degraded patchiness reduces microbial necromass content but increases contribution to soil organic carbon accumulation. Sci. Total Environ. 951. http://doi.org/10.1016/j.scitotenv.2024.175717.

Bai, X., Dippold M.A., An S., Wang B., Zhang H., Loeppmann S. 2021. Extracellular enzyme activity and stoichiometry: The effect of soil microbial element limitation during leaf litter decomposition. Ecol. Indic. 121. http://doi.org/10.1016/j.ecolind.2020.107200.

Begill, N., Don A., Poeplau C. 2023. No detectable upper limit of mineral-associated organic carbon in temperate agricultural soils. Global Change Biol. 29, 4662-4669. http://doi.org/10.1111/gcb.16804.

Boeraeve, M., Honnay O., Jacquemyn H. 2018. Effects of host species, environmental filtering and forest

age on community assembly of ectomycorrhizal fungi in fragmented forests. Fungal Ecol. 36, 89-98. http://doi.org/10.1016/j.funeco.2018.08.003.

Bossio, D.A., Scow K.M. 1998. Impacts of carbon and flooding on soil microbial communities: Phospholipid fatty acid profiles and substrate utilization patterns. Microbial Ecol. 35, 265-278. http://doi.org/10.1007/s002489900082.

Cheeke, T.E., Phillips R.P., Brzostek E.R., Rosling A., Bever J.D., Fransson P. 2017. Dominant mycorrhizal association of trees alters carbon and nutrient cycling by selecting for microbial groups with distinct enzyme function. New Phytol. 214, 432-442. http://doi.org/10.1111/nph.14343.

Chen, G., Ma S., Tian D., Xiao W., Jiang L., Xing A., Zou A., Zhou L., Shen H., Zheng C., Ji C., He H., Zhu B., Liu L., Fang J. 2020. Patterns and determinants of soil microbial residues from tropical to boreal forests. Soil Biol. & Biochem. 151. http://doi.org/10.1016/j.soilbio.2020.108059.

Cheng, X., Zhang Y., Xing W. 2024. Soil bacterial habitat generalists strengthen depth-dependent organic carbon accrual in coastal reclaimed lands after afforestation. Catena. 234,http://doi.org/10.1016/j.catena.2023.107584.

Cotrufo, M.F., Ranalli M.G., Haddix M.L., Six J., Lugato E. 2019. Soil carbon storage informed by particulate and mineral-associated organic matter. Nat. Geoscience. 12, 989. http://doi.org/10.1038/s41561-019-0484-6.

Cui, Y., Bing H., Fang L., Jiang M., Shen G., Yu J., Wang X., Zhu H., Wu Y., Zhang X. 2021. Extracellular enzyme stoichiometry reveals the carbon and phosphorus limitations of microbial metabolisms in the rhizosphere and bulk soils in alpine ecosystems. Plant and Soil. 458, 7-20. http://doi.org/10.1007/s11104-019-04159-x.

Dalal, R.C. 1998. Soil microbial biomass - what do the numbers really mean? Aust. J. Exp. Agr. 38, 649-665. http://doi.org/10.1071/ea97142.

Della Maggiora, L., Francini A., Giovannelli A., Sebastiani L. 2023. Assessment of the salinity tolerance, response mechanisms and nutritional imbalance to heterogeneous salt supply in *Populus alba* L. clone 'Marte' using a split-root system. Plant Growth Regul. 101, 251-265. http://doi.org/10.1007/s10725-023-01017-w.

Don, A., Schumacher J., Freibauer A. 2011. Impact of tropical land-use change on soil organic carbon stocks-a meta-analysis. Global Change Biol. 17, 1658-1670. http://doi.org/10.1111/j.1365-2486.2010.02336.x.

Du, Y., Wei Y., Zhou Y., Wang Y., Zhang A., Wang T., Li Z. 2024. Temporal variation of microbial nutrient limitation in citrus plantations: Insights from soil enzyme stoichiometry. Environ Res. 258. http://doi.org/10.1016/j.envres.2024.119275.

Du, Y., Zhang Y., Zhang Z., Gao Y., Mu Z., Islam W., Zeng F. 2025. Nutrient and stoichiometric characteristics of various organs in three typical desert plants from extreme desert ecosystems. Rhizosphere. 33. http://doi.org/10.1016/j.rhisph.2025.101025.

Frey, D.W., Kebede E., Sparks J.P., Fahey T.J., Goodale C.L. 2025. Increased soil nitrogen availability suppresses annual soil respiration in mixed temperate forests regardless of acidification. Global Change Biol. 31. http://doi.org/10.1111/gcb.70140.

Gao, Y., Tariq A., Zeng F., Graciano C., Zhang Z., Sardans J., Penuelas J. 2022a. Allocation of foliar-P fractions of *Alhagi sparsifolia* and its relationship with soil-P fractions and soil properties in a hyperarid desert ecosystem. Geoderma. 407. http://doi.org/10.1016/j.geoderma.2021.115546.

Gao, Y., Tariq A., Zeng F., Sardans J., Al-Bakre D.A., Penuelas J. 2024. Fractions of soil phosphorus

mediated by rhizospheric *phoD*-harbouring bacteria of deep-rooted desert species are determined by fine-root traits. Functional Ecology. 38, 2300-2315. http://doi.org/10.1111/1365-2435.14635.

Gao, Y., Tariq A., Zeng F., Sardans J., Zhang Z., Islam W., Xu M., Penuelas J. 2022b. "Fertile islands" beneath three desert vegetation on soil phosphorus fractions, enzymatic activities, and microbial biomass in the desert-oasis transition zone. Catena. 212,http://doi.org/10.1016/j.catena.2022.106090.

Ghani, M.I., Wang J., Li P., Pathan S.I., Sial T.A., Datta R., Mokhtar A., Ali E.F., Rinklebe J., Shaheen S.M., Liu M., Abdelrahman H. 2023. Variations of soil organic carbon fractions in response to conservative vegetation successions on the Loess Plateau of China. Int Soil and Water Conse. 11, 561-571. http://doi.org/10.1016/j.iswcr.2022.05.002.

Gu, R., Xiao K., Zhu Z., He X., Li D. 2024. Afforestation enhances glomalin-related soil protein content but decreases its contribution to soil organic carbon in a subtropical karst area. J. Environ. Manage. 356,http://doi.org/10.1016/j.jenvman.2024.120754.

Hansen, P.M., Even R., King A.E., Lavallee J., Schipanski M., Cotrufo M.F. 2024. Distinct, direct and climate-mediated environmental controls on global particulate and mineral-associated organic carbon storage. Global Change Biol. 30,http://doi.org/10.1111/gcb.17080.

Hassink, J. 1997. The capacity of soils to preserve organic C and N by their association with clay and silt particles. Plant and Soil. 191, 77-87. http://doi.org/10.1023/a:1004213929699.

Heckman, K., Pries C.E.H., Lawrence C.R., Rasmussen C., Crow S.E., Hoyt A.M., von Fromm S.F., Shi Z., Stoner S., McGrath C., Beem-Miller J., Berhe A.A., Blankinship J.C., Keiluweit M., Marin-Spiotta E., Monroe J.G., Plante A.F., Schimel J., Sierra C.A., Thompson A., Wagai R. 2022. Beyond bulk: Density fractions explain heterogeneity in global soil carbon abundance and persistence. Global Change Biol. 28, 1178-1196. http://doi.org/10.1111/gcb.16023.

Hong, S., Yin G., Piao S., Dybzinski R., Cong N., Li X., Wang K., Penuelas J., Zeng H., Chen A. 2020. Divergent responses of soil organic carbon to afforestation. Nat. Sustain. 3, 694. http://doi.org/10.1038/s41893-020-0557-y.

Hook, P.B., Burke I.C. 2000. Biogeochemistry in a shortgrass landscape: Control by topography, soil texture, and microclimate. Ecology. 81, 2686-2703. http://doi.org/10.1890/0012-9658(2000)081[2686:Biaslc]2.0.Co;2.

Jackson, R.B., Lajtha K., Crow S.E., Hugelius G., Kramer M.G., Pineiro G. 2017. The ecology of soil carbon: pools, vulnerabilities, and biotic and abiotic controls. Annual Rev. Ecol. Evol. S. 48: 419-445. http://doi.org/ 210.1146/annurev-ecolsys-112414-054234.

Ji, Y., Zhou G., Li Z., Wang S., Zhou H., Song X. 2020. Triggers of widespread dieback and mortality of poplar (*Populus* spp.) plantations across northern China. J. Arid Environ. 174. http://doi.org/10.1016/j.jaridenv.2019.104076.

Kaiser, K., Guggenberger G., Haumaier L. 2004. Changes in dissolved lignin-derived phenols, neutral sugars, uronic acids, and amino sugars with depth in forested Haplic Arenosols and Rendzic Leptosols. Biogeochemistry. 70, 135-151. http://doi.org/10.1023/b:Biog.0000049340.77963.18.

Keiluweit, M., Bougoure J.J., Nico P.S., Pett-Ridge J., Weber P.K., Kleber M. 2015. Mineral protection of soil carbon counteracted by root exudates. Nat. Clim. Change. 5, 588-595. http://doi.org/10.1038/nclimate2580.

Kleber, M., Eusterhues K., Keiluweit M., Mikutta C., Mikutta R., Nico P.S. Mineral-organic associations: formation, properties, and relevance in soil environments .2015. Adv. Agron. 130: 1-140.

http://doi.org/10.1016/bs.agron.2014.10.005.
Kong, W., Wei X., Wu Y., Shao M., Zhang Q., Sadowsky M.J., Ishii S., Reich P.B., Wei G., Jiao S., Qiu L., Liu L. 2022. Afforestation can lower microbial diversity and functionality in deep soil layers in a semiarid region. Global Change Biol. 28, 6086-6101. http://doi.org/10.1111/gcb.16334.
Kreyling, J. 2025. Space-for-time substitution misleads projections of plant community and stand-structure development after disturbance in a slow-growing environment. J. Ecol. 113, 68-80. http://doi.org/10.1111/1365-2745.14438.
Lettens, S., van Orshoven J., van Wesemael B., Muys B., Perrin D. 2005. Soil organic carbon changes in landscape units of Belgium between 1960 and 2000 with reference to 1990. Global Change Biol. 11,2128-2140. http://doi.org/10.1111/j.1365-2486.2005.001074.x.
Li, S., Huang X., Tang R., Li J., Zhu B., Su J. 2023a. Soil microbial diversity and network complexity sustain ecosystem multifunctionality following afforestation in a dry-hot valley savanna. Catena. 231,http://doi.org/10.1016/j.catena.2023.107329.
Li, X., Yang T., Hicks L.C., Hu B., Li F., Liu X., Wei D., Wang Z., Bao W. 2023b. Latitudinal patterns of particulate and mineral-associated organic matter down the soil profile in drylands. Soil Till. Res. 226. http://doi.org/10.1016/j.still.2022.105580.
Li, Y., Zhang X., Wang B., Wu X., Wang Z., Liu L., Yang H. 2023c. Revegetation promotes soil mineral-associated organic carbon sequestration and soil carbon stability in the Tengger Desert, northern China. Soil Biol. Biochem. 185. http://doi.org/10.1016/j.soilbio.2023.109155.
Liang, C., Schimel J.P., Jastrow J.D. 2017. The importance of anabolism in microbial control over soil carbon storage. Nat. Microbiol. 2. http://doi.org/10.1038/nmicrobiol.2017.105.
Liang, Y., Fu R., Sailike A., Hao H., Yu Z., Wang R., Peng N., Li S., Zhang W., Liu Y. 2025. Soil labile organic carbon and nitrate nitrogen are the main factors driving carbon-fixing pathways during vegetation restoration in the Loess Plateau, China. Agr. Ecosyst. Environ. 378. http://doi.org/10.1016/j.agee.2024.109283.
Lin, S., Zhou Y., Wang W., Sardans J., Li Y., Fu C., Zeng F., Song Z., Tariq A., Penuelas J. 2024. Losses and destabilization of soil organic carbon stocks in coastal wetlands converted into aquaculture ponds. Global Change Biol. 30. http://doi.org/10.1111/gcb.17480.
Liu, X., Yang T., Wang Q., Huang F., Li L. 2018. Dynamics of soil carbon and nitrogen stocks after afforestation in arid and semi-arid regions: A meta-analysis. Sci. Total Environ. 618, 1658-1664. http://doi.org/10.1016/j.scitotenv.2017.10.009.
Liu, Y., Zhu G., Hai X., Li J., Shangguan Z., Peng C., Deng L. 2020. Long-term forest succession improves plant diversity and soil quality but not significantly increase soil microbial diversity: Evidence from the Loess Plateau. Ecol. Eng. 142. http://doi.org/10.1016/j.ecoleng.2019.105631.
Luo, X., Hou E., Zhang L., Zang X., Yi Y., Zhang G., Wen D. 2019. Effects of forest conversion on carbon-degrading enzyme activities in subtropical China. Sci. Total Environ. 696. http://doi.org/10.1016/j.scitotenv.2019.133968.
Moorhead, D.L., Sinsabaugh R.L., Hill B.H., Weintraub M.N. 2016. Vector analysis of ecoenzyme activities reveal constraints on coupled C, N and P dynamics. Soil Biol. Biochem. 93, 1-7. http://doi.org/10.1016/j.soilbio.2015.10.019.
Mooshammer, M., Wanek W., Haemmerle I., Fuchslueger L., Hofhansl F., Knoltsch A., Schnecker J., Takriti M., Watzka M., Wild B., Keiblinger K.M., Zechmeister-Boltenstern S., Richter A. 2014. Adjustment of microbial nitrogen use efficiency to carbon: nitrogen imbalances regulates soil nitrogen cycling. Nat. Commun. 5. http://doi.org/10.1038/ncomms4694.

Ning, S., He X., Ma T., Yan T. 2024. Attenuated asymmetry of above- versus belowground stoichiometry to a decadal nitrogen addition during stand development. Ecology. 105. http://doi.org/10.1002/ecy.4458.

Phillips, R.P., Brzostek E., Midgley M.G. 2013. The mycorrhizal-associated nutrient economy: a new framework for predicting carbon-nutrient couplings in temperate forests. New Phytol. 199. 41-51. http://doi.org/10.1111/nph.12221.

Pulleman, M.M., de Boer W., Giller K.E., Kuyper T.W. 2022. Soil biodiversity and nature-mimicry in agriculture; the power of metaphor? Outlook Agr. 51: 75-90. http://doi.org/10.1177/00307270221080180.

Rohatyn, S., Yakir D., Rotenberg E., Carmel Y. 2022. Limited climate change mitigation potential through forestation of the vast dryland regions. Science. 377.1436-1439. http://doi.org/10.1126/science.abm9684.

Sacca, M.L., Francesco C., Enrico C., Flavio F. 2024. Fungal β-glucosidase gene and corresponding enzyme activity are positively related to soil organic carbon in unmanaged woody plantations. Soil Ecol. Lett. 6. http://doi.org/10.1007/s42832-024-0238-2.

Sharma, S., Singh P., Gupta N., Utreja D., Kasana R.C. 2024. Bacterial diversity and enzymatic activities in poplar chronosequence: Implications for soil carbon dynamics in a semi-arid ecosystem. Forest Ecol. Manag. 562. http://doi.org/10.1016/j.foreco.2024.121933.

Sinsabaugh, R.L., Shah J.J.F. 2011. Ecoenzymatic stoichiometry of recalcitrant organic matter decomposition: the growth rate hypothesis in reverse. Biogeochemistry. 102: 31-43. http://doi.org/10.1007/s10533-010-9482-x.

Six, J., Callewaert P., Lenders S., De Gryze S., Morris S.J., Gregorich E.G., Paul E.A., Paustian K. 2002a. Measuring and understanding carbon storage in afforested soils by physical fractionation. Soil Sci. Soc. Am. J. 66: 1981-1987. http://doi.org/10.2136/sssaj2002.1981.

Six, J., Conant R.T., Paul E.A., Paustian K. 2002b. Stabilization mechanisms of soil organic matter: Implications for C-saturation of soils. Plant and Soil. 241: 155-176. http://doi.org/10.1023/a:1016125726789.

Sokol, N.W., Sanderman J., Bradford M.A. 2019. Pathways of mineral-associated soil organic matter formation: Integrating the role of plant carbon source, chemistry, and point of entry. Global Change Biol. 25:12-24. http://doi.org/10.1111/gcb.14482.

Stewart, C.E., Paustian K., Conant R.T., Plante A.F., Six J. 2007. Soil carbon saturation: concept, evidence and evaluation. Biogeochemistry. 86,19-31. http://doi.org/10.1007/s10533-007-9140-0.

Su, Z., Zhong Y., Zhu X., Wu Y., Shen Z., Shangguan Z. 2023. Vegetation restoration altered the soil organic carbon composition and favoured its stability in a *Robinia pseudoacacia* plantation. Sci. Total Environ. 899. http://doi.org/10.1016/j.scitotenv.2023.165665.

Tang, Q., Li W., Wang J., Zhang F., Dai W., Li Z., Wang S., Yin W., Cheng Y., Wang X. 2025. Coupled iron oxides and microbial-mediated soil organic carbon stabilization across tea plantation chronosequences. Soil Till. Res. 247. http://doi.org/10.1016/j.still.2024.106382.

Tariq, A., Sardans J., Zeng F.J., Graciano C., Hughes A.C., Farré-Armengol G., Peñuelas J. 2024. Impact of aridity rise and arid lands expansion on carbon-storing capacity, biodiversity loss, and ecosystem services. Global Change Biol. 30. http://doi.org/10.1111/gcb.17292.

Villarino, S.H., Pinto P., Jackson R.B., Piñeiro G. 2021. Plant rhizodeposition: A key factor for soil organic matter formation in stable fractions. Sci. Adv. 7. http://doi.org/10.1126/sciadv.abd3176.

Wang, B., An S., Liang C., Liu Y., Kuzyakov Y. 2021. Microbial necromass as the source of soil organic carbon in global ecosystems. Soil Biol. Biochem 162. http://doi.org/10.1016/j.soilbio.2021.108422.

Wang, G., Xiao H.J., Xin Z.M., Luo F.M., Jin Y.X., Liu M.M., Li J.R. 2024a. Changes in plant-soil-microbe C-N-P contents and stoichiometry during poplar shelterbelt degradation. Catena. 243. http://doi.org/10.1016/j.catena.2024.108227.

Wang, J., Wang X., Liu G., Wang G., Wu Y., Zhang C. 2020. Fencing as an effective approach for restoration of alpine meadows: Evidence from nutrient limitation of soil microbes. Geoderma. 363. http://doi.org/10.1016/j.geoderma.2019.114148.

Wang, Y., Zhai D., Cheng X. 2024b. Soil nitrogen and phosphorus dynamics respond divergently to afforestation. Forest Ecol. Manag. 555. http://doi.org/10.1016/j.foreco.2024.121705.

Willard, S.J., Liang G.P., Adkins S., Foley K., Murray J., Waring B. 2024. Land use drives the distribution of free, physically protected, and chemically protected soil organic carbon storage at a global scale. Global Change Biol. 30. http://doi.org/10.1111/gcb.17507.

Witzgall, K., Vidal A., Schubert D.I., Hoeschen C., Schweizer S.A., Buegger F., Pouteau V., Chenu C., Mueller C.W. 2021. Particulate organic matter as a functional soil component for persistent soil organic carbon. Nat. Commun. 12. http://doi.org/10.1038/s41467-021-24192-8.

Xi, B., Clothier B., Coleman M., Duan J., Hu W., Li D., Di N., Liu Y., Fu J., Li J., Jia L., Fernandez J.-E. 2021. Irrigation management in poplar (*Populus* spp.) plantations: A review. Forest Ecol. and Manag. 494. http://doi.org/10.1016/j.foreco.2021.119330.

Yang, X., Ren W., Sun B., Zhang S. 2012. Effects of contrasting soil management regimes on total and labile soil organic carbon fractions in a loess soil in China. Geoderma. 177. 49-56. http://doi.org/10.1016/j.geoderma.2012.01.033.

Yu, P., Li Y., Liu S., Liu J., Ding Z., Ma M., Tang X. 2022. Afforestation influences soil organic carbon and its fractions associated with aggregates in a karst region of Southwest China. Sci. Total Environ. 814. http://doi.org/10.1016/j.scitotenv.2021.152710.

Zhang, H., Liu G., Wu J. 2024a. The effect of land degradation and restoration on particulate and mineral-associated organic carbon. Appl. Soil Ecol. 196. http://doi.org/10.1016/j.apsoil.2024.105322.

Zhang, Z., Cong M., Zhao G., Song J., Du Y., Zhang Y., Dong X., Tariq A., Wang W., Zeng F. 2024b. Soil microbial community dynamics in response to *Tamarix ramosissima* afforestation in desert lands: Metagenomic insights. Land Degrad. Dev. 35: 4133-4144. http://doi.org/10.1002/ldr.5210.

Zhang, Z., Tariq A., Zeng F., Graciano C., Zhang B. 2020. Nitrogen application mitigates drought-induced metabolic changes in *Alhagi sparsifolia* seedlings by regulating nutrient and biomass allocation patterns. Plant Physiol. and Bioch. 155: 828-841. http://doi.org/10.1016/j.plaphy.2020.08.036.

Zhao, G., Tariq A., Zhang Z., Nazim M., Graciano C., Sardans J., Dong X., Gao Y., Penuelas J., Zeng F. 2025a. Afforestation with xerophytic shrubs promoted soil organic carbon stability in a hyper-arid environment of desert. Land Degrad. Dev. 36: 655-667. http://doi.org/10.1002/ldr.5387.

Zhao, G., Zhang Z., Tariq A., Sabit R., Sardans J., Graciano C., Li X., Zhu Y., Penuelas J., Al-Bakre D.A., Zeng F. 2025b. Grazing exclusion significantly reduced soil organic carbon stocks but enhanced soil inorganic carbon stocks in desert steppe of northwest China. Ecol. Indic. 172. http://doi.org/10.1016/j.ecolind.2025.113341.

Zheng, H., Hede P., Rousk J., Schmidt I.K., Peng Y., Vesterdal L. 2022. Effects of common European

tree species on soil microbial resource limitation, microbial communities and soil carbon. Soil Biol Biochem. 172. http://doi.org/10.1016/j.soilbio.2022.108754.

Figure caption

Fig. 1 General view of the research sites. PH: plant height. DBH: diameter at breast height.

Fig. 2 Effects of afforestation on the concentration of SOC and fractions. The error bars are the standard deviation (n=4). Different lowercase letters indicate significant differences stand ages at $P < 0.05$ for individual variables, and different uppercase letters denote significant differences between topsoil and subsoil at $P < 0.05$ for individual variables. Y: Stand ages; D: Soil depth.

Fig. 3 Effects of afforestation on SOC stability index. The error bars are the standard deviation (n=4). Different lowercase letters indicate significant differences stand ages at $P < 0.05$ for individual variables, and different uppercase letters denote significant differences between topsoil and subsoil at $P < 0.05$ for individual variables. Y: Stand ages; D: Soil depth.

Fig. 4 Effects of afforestation on abundance and ratios of soil microbial groups as indicated by phospholipid fatty acids (PLFAs). GP, Gram-positive bacteria; GN, Gram-negative bacteria; F/B, Ratio of fungi to bacteria. The error bars are the standard deviation (n=4). Different lowercase letters indicate significant differences stand ages at $P < 0.05$ for individual variables, and different uppercase letters denote significant differences between topsoil and subsoil at $P < 0.05$ for individual variables. Y: Stand ages; D: Soil depth.

Fig. 5 Microbial metabolic limitations indicated by extracellular enzymatic stoichiometry (a-d): (a) A high vector length implies more microbial C limitation; (b) A vector angle higher than 45° represents the P limitation and conversely represents the N limitation; (c) vector analysis (vector length and angle); horizontal and vertical baseline chemometric analysis. The error bars are the standard deviation (n=4). Different lowercase letters indicate significant differences stand ages at $P < 0.05$ for individual variables, and different uppercase letters denote significant differences between topsoil and subsoil at $P < 0.05$ for individual variables. Y: Stand ages; D: Soil depth. A vector angle of <45° denotes N limitation (red horizontal dashed line), and angles >45° denote P limitation. By using 1.0 as the baseline along both the horizontal and vertical axes of enzyme activity ratios ((NAG+LAP)/ALP as the x-axis and (BG+CBH) /(NAG+LAP) as the y-axis). Four distinct groups of microbial resource limitations were identified: N limitation, P limitation, C and N colimitation, and C and P colimitation. Nearly all treatment are clearly P, C and P limited (light red shaded area).

Fig. 6 Heatmap and random forest showed the effects of vegetation characteristics, soil physicochemical properties, microbial limitation, and PLFAs contribution to SOC (a) and SI (b). *$P < 0.05$, **$P < 0.01$, ***$P < 0.001$. EC, electrical conductivity; TN, total nitrogen; TP, total phosphorus; TK, total potassium; NO_3^--N, nitrate nitrogen; NH_4^+-N, ammonium nitrogen; AP, available phosphorus; AK, available potassium.

Fig. 7 Partial least squares path modeling (PLS-PM) showing the effects of afforestation on the concentration of SOC (a) and SI (b) and standardized total effects of environmental variables derived from the PLS-PM (c, d). Red arrows represent negative relationships, and blue arrows represent positive relationships. The solid arrows represent significant relationships (*$P < 0.05$, **$P < 0.01$, ***$P < 0.001$), and the gray dashed arrows represent nonsignificant relationships. The width of the arrow represents the size of the path coefficient. GOF, goodness of fit.

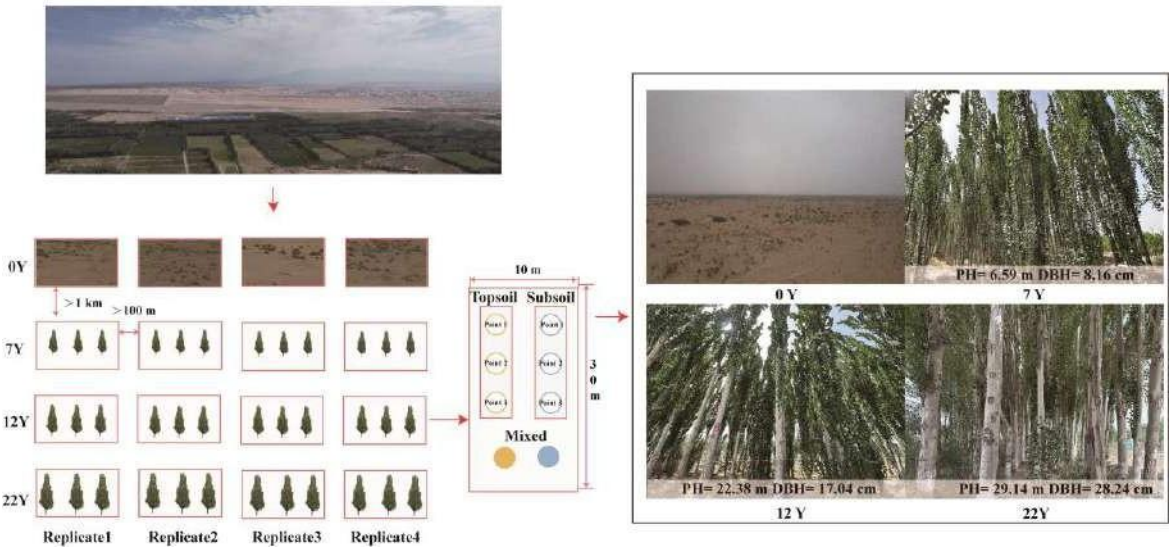
0Y
>1 km
>100 m
7Y
12Y
22Y
Replicate1
Replicate2
Replicate3
Replicate4
10 m
Topsoil
Subsoil
30 m
Mixed
0 Y
7 Y
PH= 6.59 m DBH= 8.16 cm
PH= 22.38 m DBH= 17.04 cm
PH= 29.14 m DBH= 28.24 cm
12 Y
22Y

Fig. 1

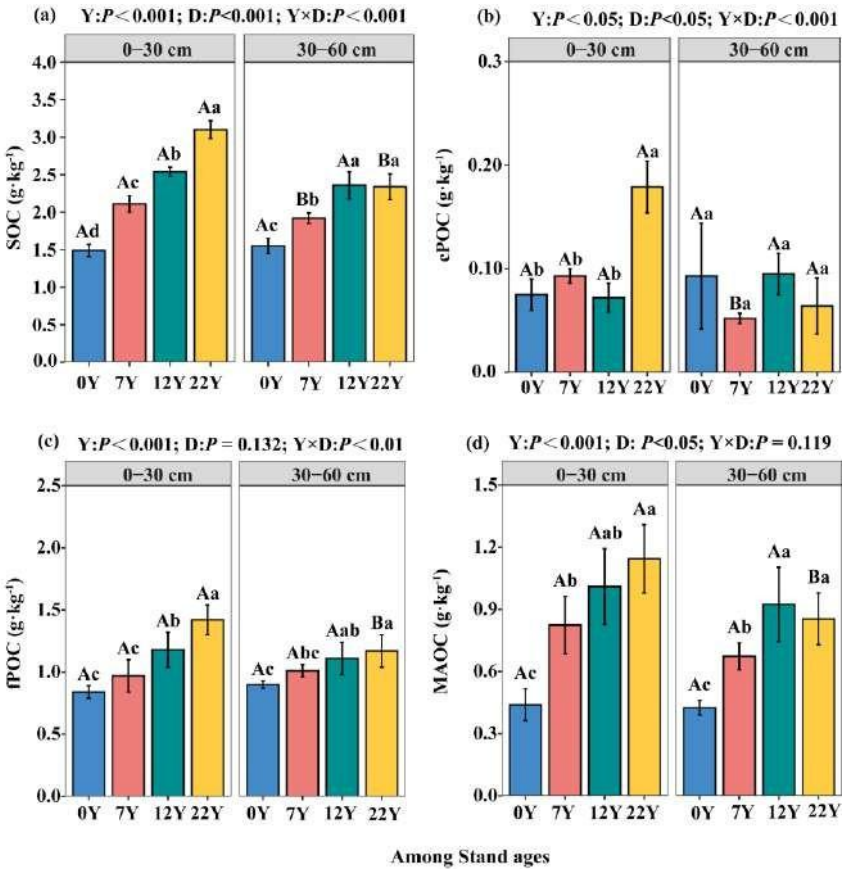
(a) Y:P < 0.001; D:P<0.001; Y×D:P < 0.001
0–30 cm
30–60 cm
SOC (g·kg⁻¹)
Ad
Ac
Ab
Aa
Ac
Bb
Aa
Ba
0Y 7Y 12Y 22Y
(b) Y:P < 0.05; D:P<0.05; Y×D:P < 0.001
cPOC (g·kg⁻¹)
Ab
Ab
Ab
Aa
Aa
Ba
Aa
Aa
(c) Y:P < 0.001; D:P = 0.132; Y×D:P < 0.01
fPOC (g·kg⁻¹)
Ac
Ac
Ab
Aa
Ac
Abc
Aab
Ba
(d) Y:P < 0.001; D: P<0.05; Y×D:P = 0.119
MAOC (g·kg⁻¹)
Ac
Ab
Aab
Aa
Ac
Ab
Aa
Ba
Among Stand ages

Fig. 2

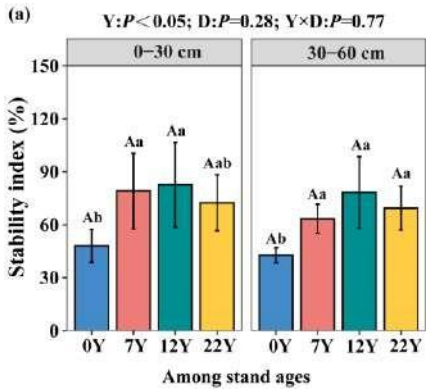

682

683 **Fig. 3**

684

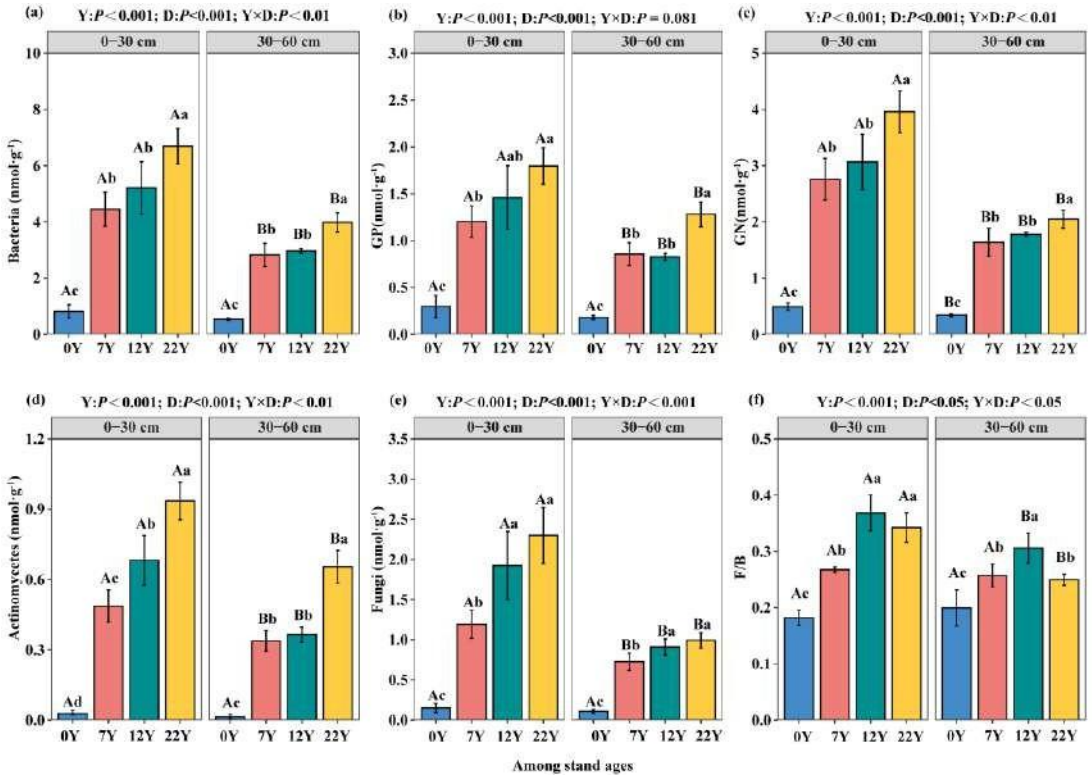
(a)
Y:P < 0.001; D:P<0.001; Y×D:P < 0.01
0–30 cm
30–60 cm
Bacteria (nmol·g⁻¹)
(b)
Y:P < 0.001; D:P<0.001; Y×D:P = 0.081
GP(nmol·g⁻¹)
(c)
Y:P < 0.001; D:P<0.001; Y×D:P < 0.01
GN(nmol·g⁻¹)
(d)
Y:P < 0.001; D:P<0.001; Y×D:P < 0.01
Actinomycetes (nmol·g⁻¹)
(e)
Y:P < 0.001; D:P<0.001; Y×D:P < 0.001
Fungi (nmol·g⁻¹)
(f)
Y:P < 0.001; D:P<0.05; Y×D:P < 0.05
F/B
0Y 7Y 12Y 22Y
Among stand ages

Fig. 4

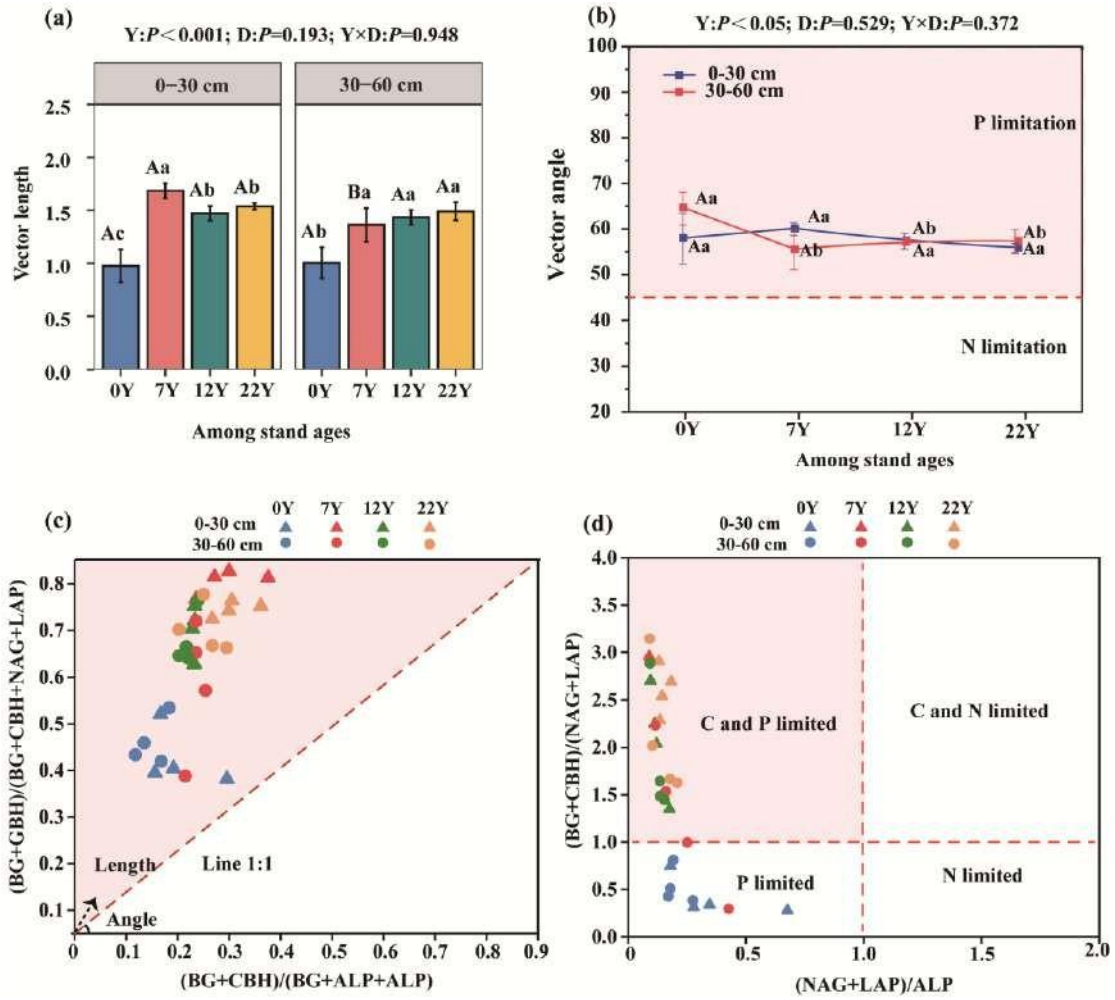
(a)
Y:P<0.001; D:P=0.193; Y×D:P=0.948
0−30 cm
30−60 cm
Vector length
Ac
Aa
Ab
Ab
Ab
Ba
Aa
Aa
0Y 7Y 12Y 22Y
Among stand ages
(b)
Y:P<0.05; D:P=0.529; Y×D:P=0.372
0-30 cm
30-60 cm
P limitation
N limitation
Vector angle
Among stand ages
(c)
0-30 cm
30-60 cm
Length
Line 1:1
Angle
(BG+GBH)/(BG+CBH+NAG+LAP)
(BG+CBH)/(BG+ALP+ALP)
(d)
C and P limited
C and N limited
P limited
N limited
(BG+CBH)/(NAG+LAP)
(NAG+LAP)/ALP

Fig. 5

691

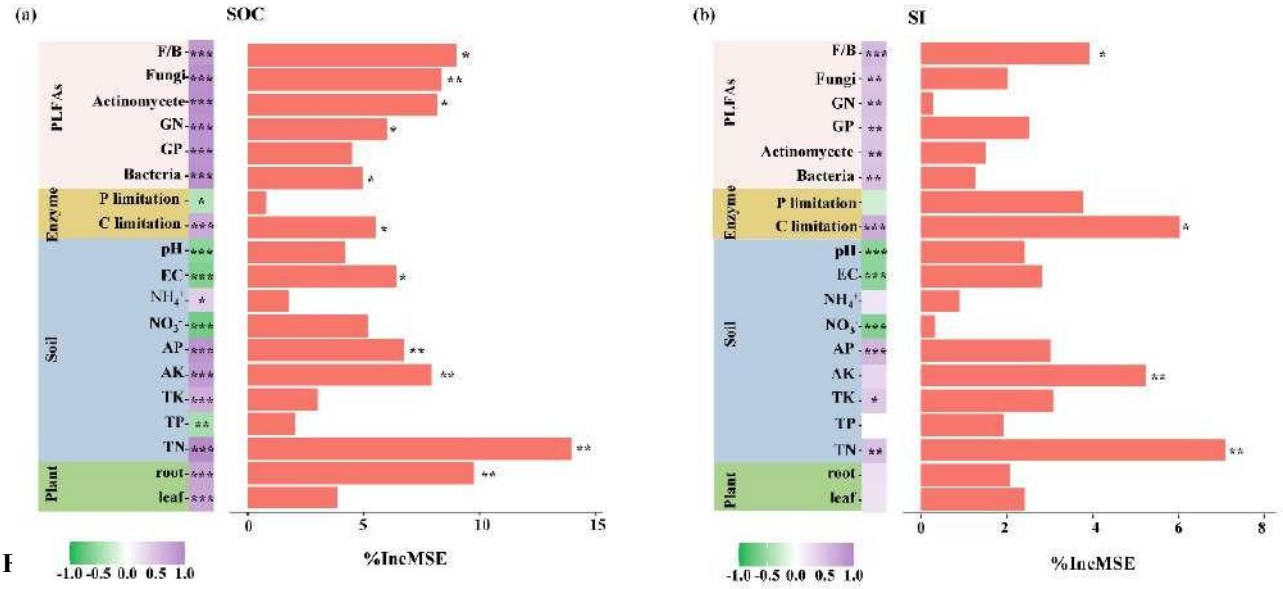

692

693 **F**

694

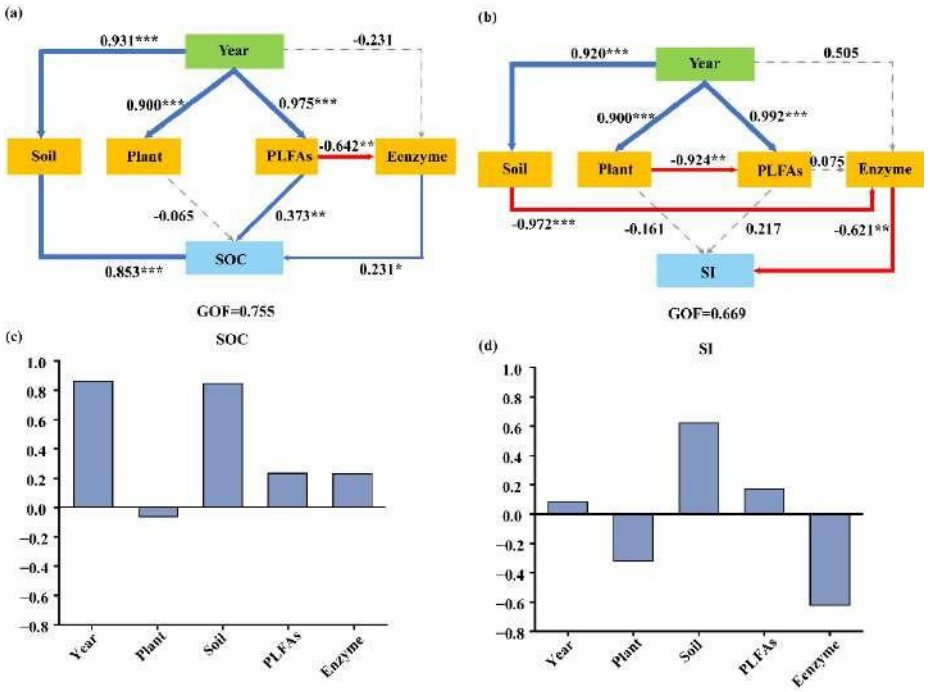
(a)
0.931***
Year
-0.231
0.900***
0.975***
Soil
Plant
PLFAs
-0.642**
Eenzyme
-0.065
0.373**
SOC
0.853***
0.231*
GOF=0.755
(b)
0.920***
Year
0.505
0.900***
0.992***
Soil
Plant
-0.924**
PLFAs
0.075
Enzyme
-0.972***
-0.161
0.217
-0.621**
SI
GOF=0.669
(c)
SOC
1.0
0.8
0.6
0.4
0.2
0.0
−0.2
−0.4
−0.6
−0.8
Year
Plant
Soil
PLFAs
Enzyme
(d)
SI
1.0
0.8
0.6
0.4
0.2
0.0
−0.2
−0.4
−0.6
−0.8
Year
Plant
Soil
PLFAs
Enzyme

Fig. **7**

Figure 1

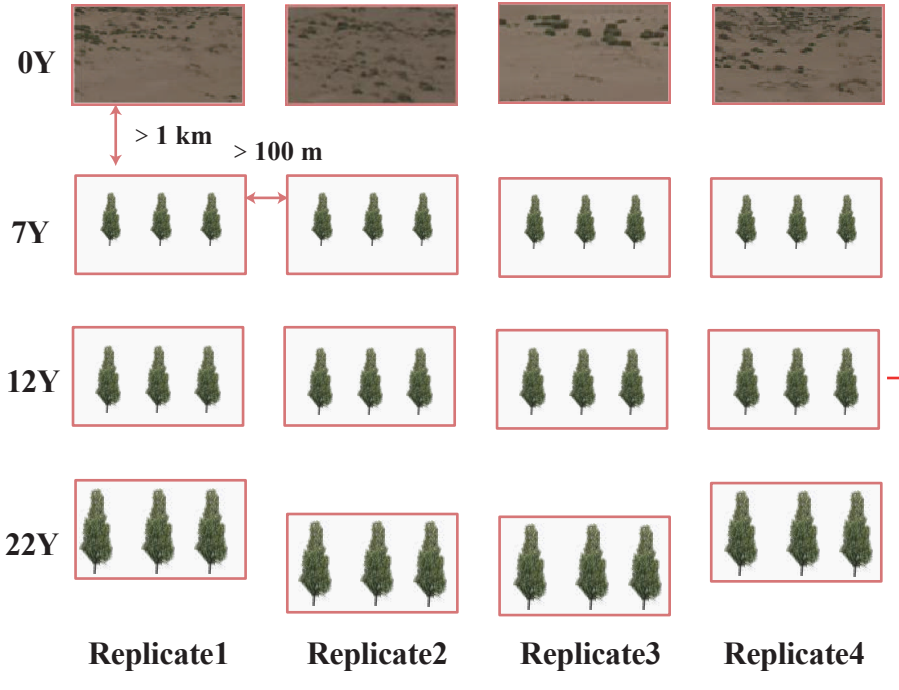
0Y
> 1 km
> 100 m
7Y
12Y
22Y
Replicate1
Replicate2
Replicate3
Replicate4

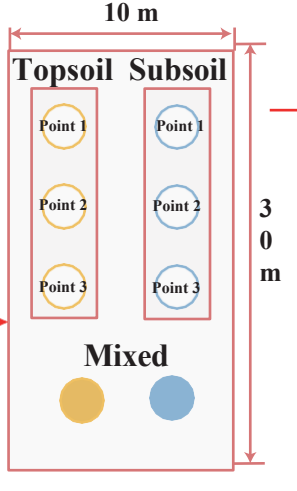
10 m
Topsoil
Subsoil
Point 1
Point 2
Point 3
Point 1
Point 2
Point 3
Mixed
3
0
m

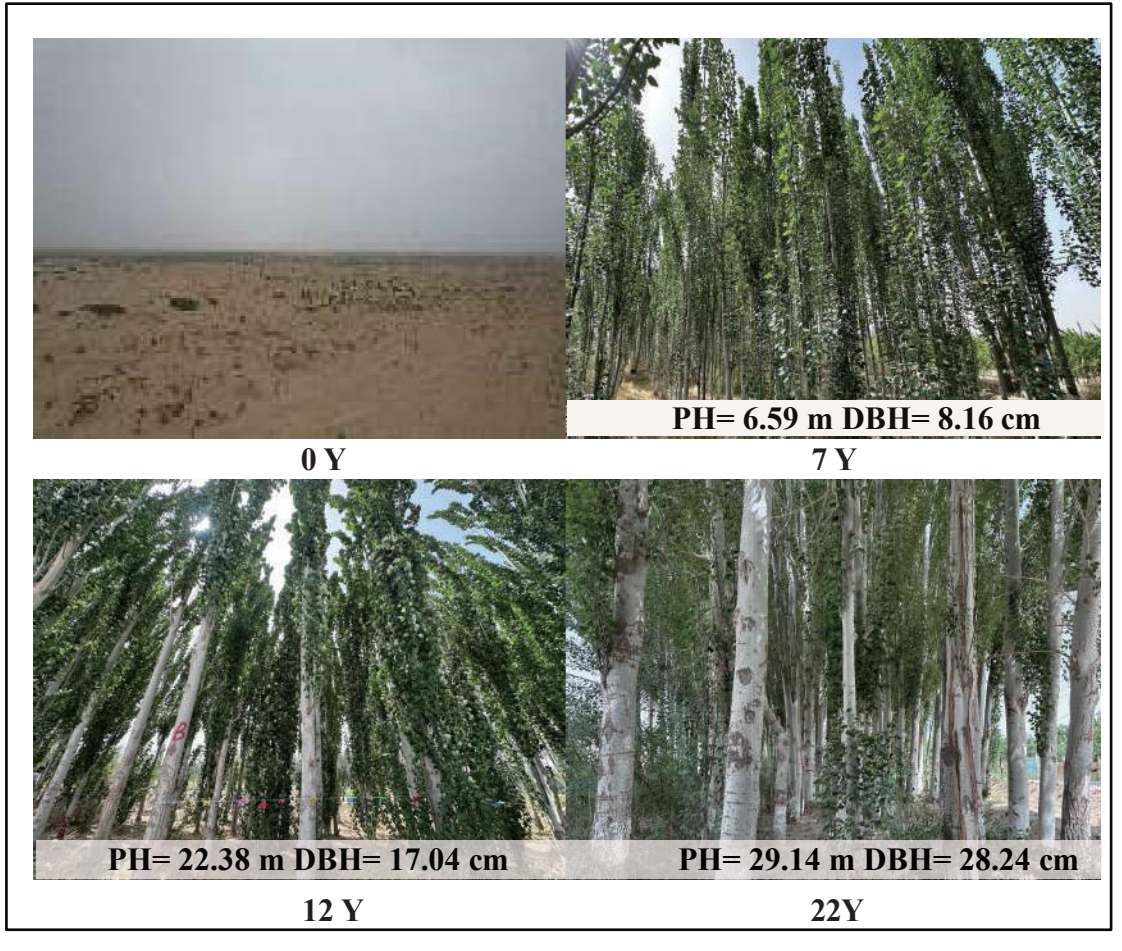
PH= 6.59 m DBH= 8.16 cm
0 Y
7 Y
PH= 22.38 m DBH= 17.04 cm
PH= 29.14 m DBH= 28.24 cm
12 Y
22Y

Figure 2

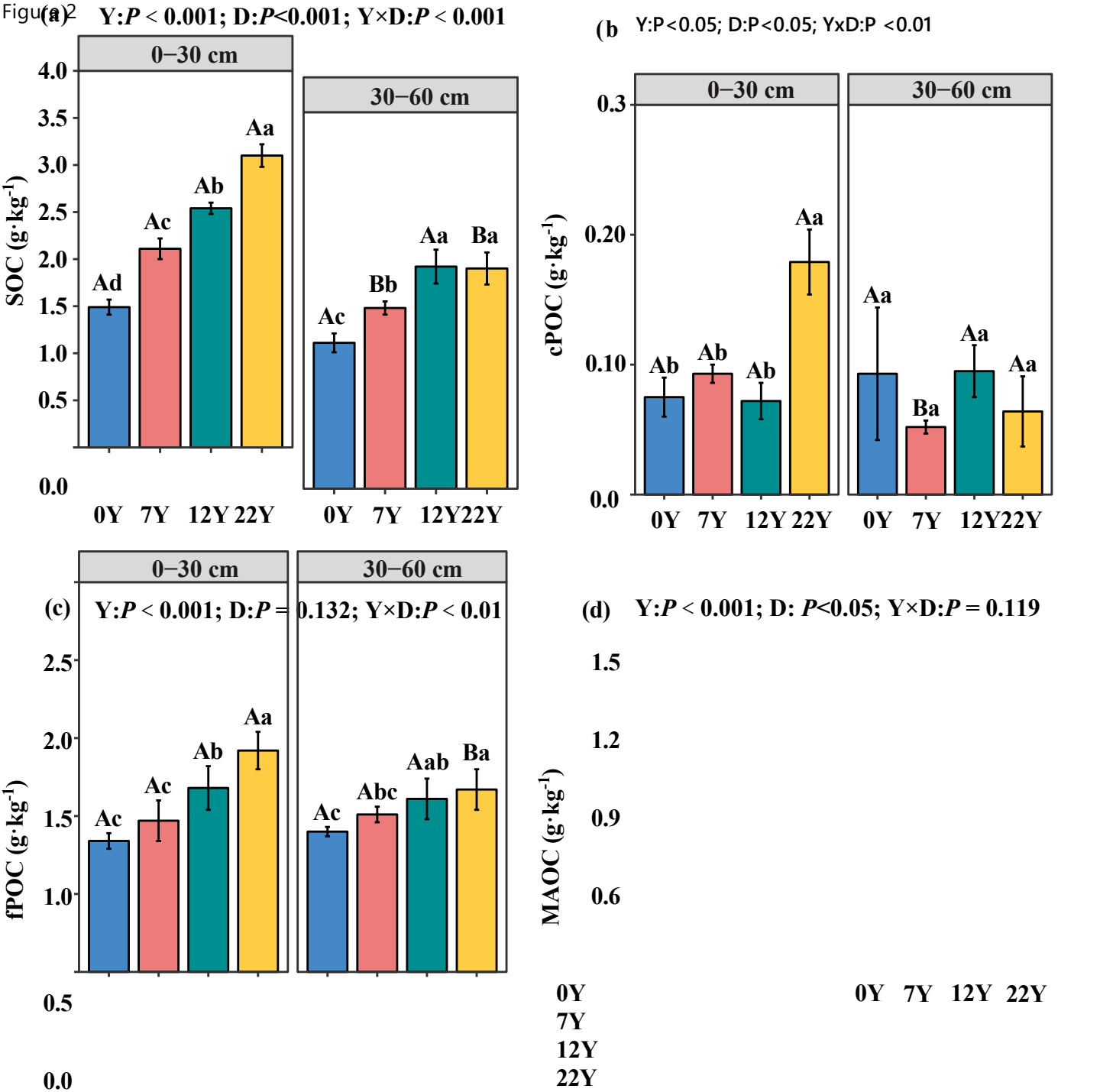
(a) Y:P < 0.001; D:P<0.001; Y×D:P < 0.001
0–30 cm
30–60 cm
SOC (g·kg-1)
4.0
3.5
3.0
2.5
2.0
1.5
1.0
0.5
0.0
Ad
Ac
Ab
Aa
Ac
Bb
Aa
Ba
0Y 7Y 12Y 22Y
0Y 7Y 12Y22Y
(b Y:P<0.05; D:P<0.05; YxD:P <0.01
0–30 cm
30–60 cm
cPOC (g·kg-1)
0.3
0.20
0.10
0.0
Ab
Ab
Ab
Aa
Aa
Ba
Aa
Aa
0Y 7Y 12Y 22Y
0Y 7Y 12Y22Y
(c) Y:P < 0.001; D:P = 0.132; Y×D:P < 0.01
0–30 cm
30–60 cm
fPOC (g·kg-1)
2.5
2.0
1.5
1.0
0.5
0.0
Ac
Ac
Ab
Aa
Ac
Abc
Aab
Ba
(d) Y:P < 0.001; D: P<0.05; Y×D:P = 0.119
MAOC (g·kg-1)
1.5
1.2
0.9
0.6
0Y
7Y
12Y
22Y
0Y 7Y 12Y 22Y

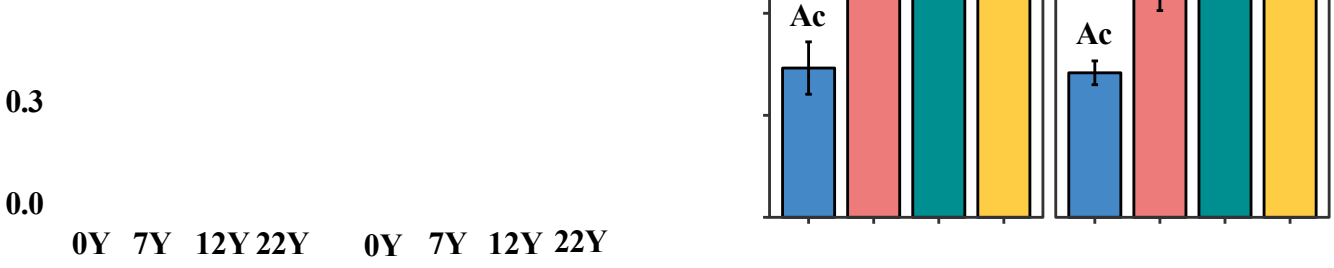
Ac
Ac
0.3
0.0
0Y 7Y 12Y 22Y
0Y 7Y 12Y 22Y
Among Stand ages

Figure 3

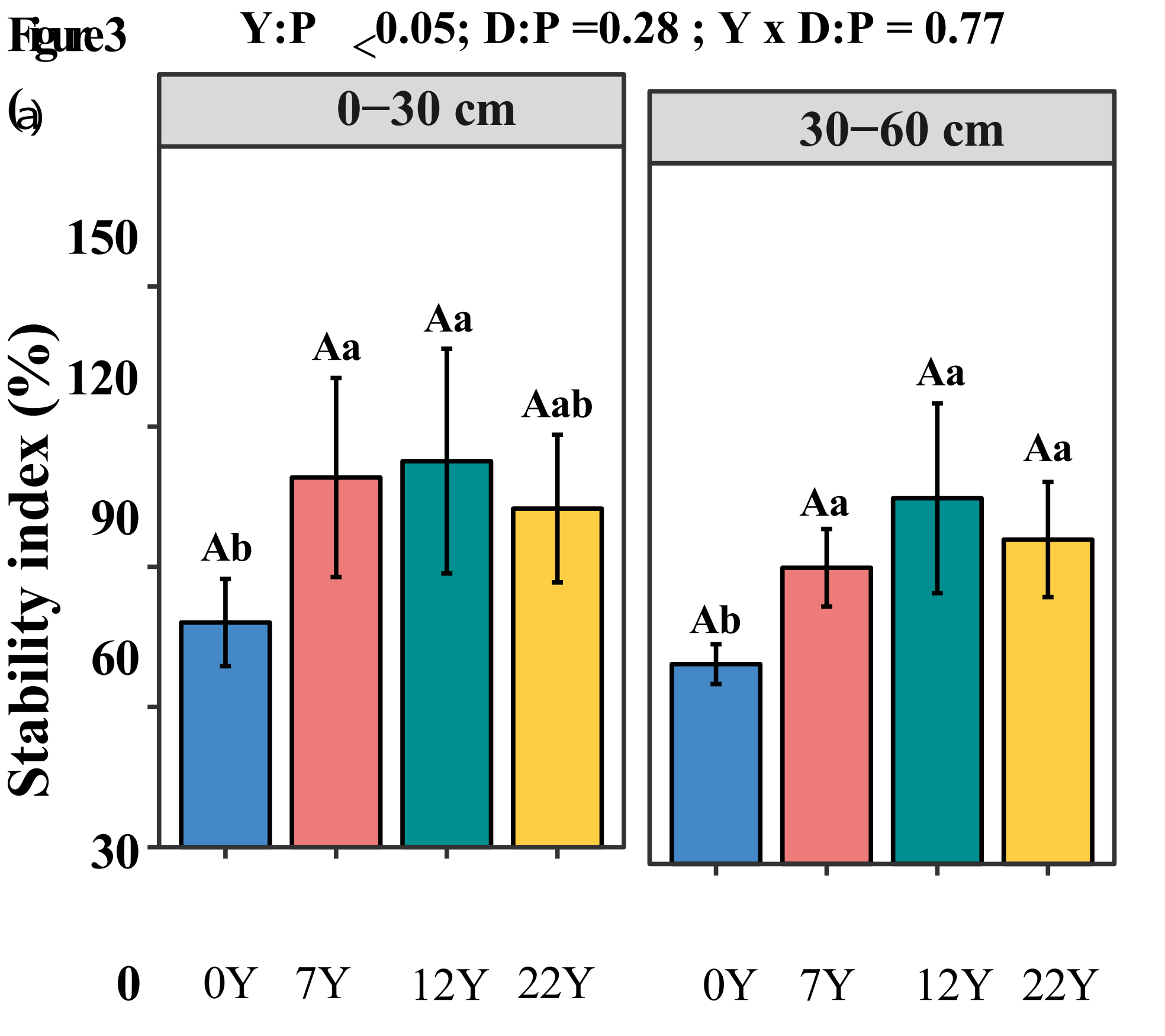
Y:P < 0.05; D:P =0.28 ; Y x D:P = 0.77
(a)
0–30 cm
30–60 cm
Stability index (%)
150
120
90
60
30
0
Ab
Aa
Aa
Aab
Ab
Aa
Aa
Aa
0Y
7Y
12Y
22Y
0Y
7Y
12Y
22Y

Among stand ages

Figure 4

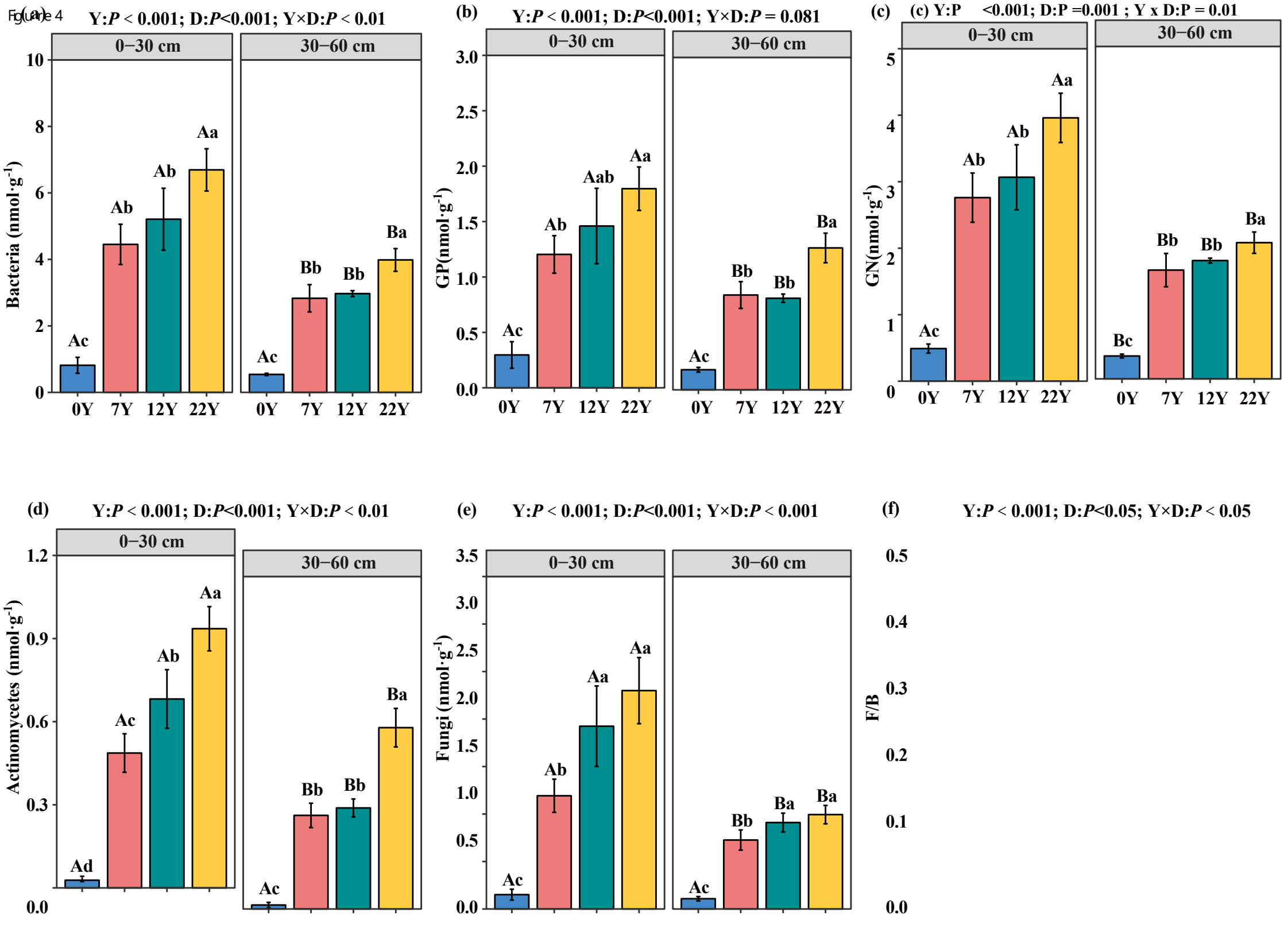
(a)
Y:P < 0.001; D:P<0.001; Y×D:P < 0.01
0–30 cm
30–60 cm
Bacteria (nmol·g-1)
Ac
Ab
Aa
Bb
Ba
0Y
7Y
12Y
22Y
(b)
Y:P < 0.001; D:P<0.001; Y×D:P = 0.081
GP(nmol·g-1)
Aab
(c)
(c) Y:P <0.001; D:P =0.001 ; Y x D:P = 0.01
GN(nmol·g-1)
Bc
(d)
Y:P < 0.001; D:P<0.001; Y×D:P < 0.01
Actinomycetes (nmol·g-1)
Ad
(e)
Y:P < 0.001; D:P<0.001; Y×D:P < 0.001
Fungi (nmol·g-1)
(f)
Y:P < 0.001; D:P<0.05; Y×D:P < 0.05
F/B

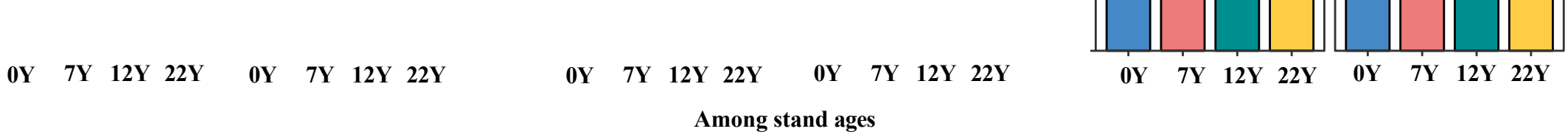
0Y 7Y 12Y 22Y
0Y 7Y 12Y 22Y
0Y 7Y 12Y 22Y
0Y 7Y 12Y 22Y
0Y 7Y 12Y 22Y
0Y 7Y 12Y 22Y
Among stand ages

Figure 5

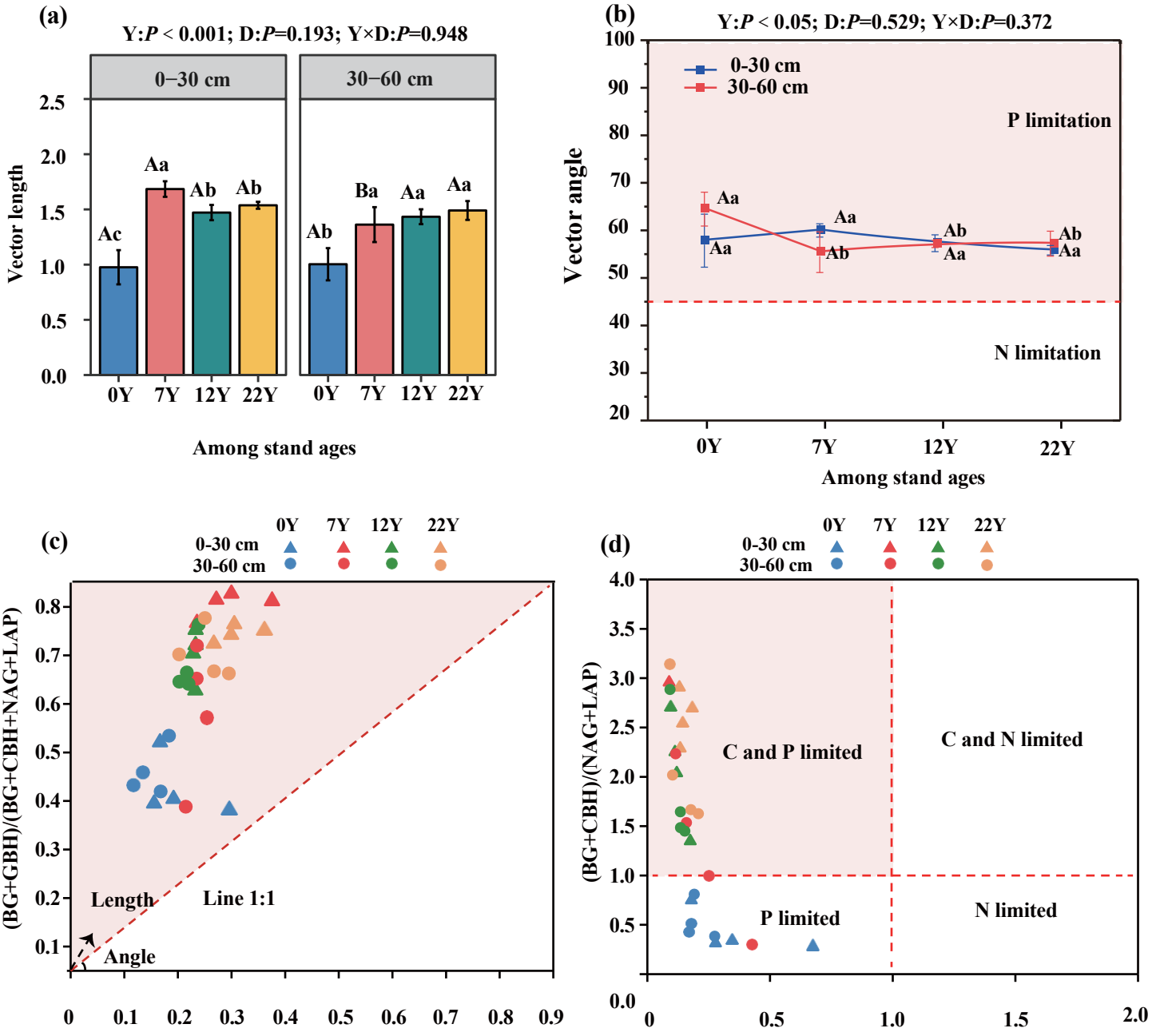
(a)
Y:P < 0.001; D:P=0.193; Y×D:P=0.948
0−30 cm
30−60 cm
Vector length
Ac
Aa
Ab
Ab
Ab
Ba
Aa
Aa
0Y
7Y
12Y
22Y
Among stand ages
(b)
Y:P < 0.05; D:P=0.529; Y×D:P=0.372
0-30 cm
30-60 cm
P limitation
N limitation
Vector angle
Among stand ages
(c)
0-30 cm
30-60 cm
(BG+GBH)/(BG+CBH+NAG+LAP)
Length
Line 1:1
Angle
(d)
C and P limited
C and N limited
P limited
N limited
(BG+CBH)/(NAG+LAP)

(BG+CBH)/(BG+ALP+ALP)

(NAG+LAP)/ALP

Figure 6

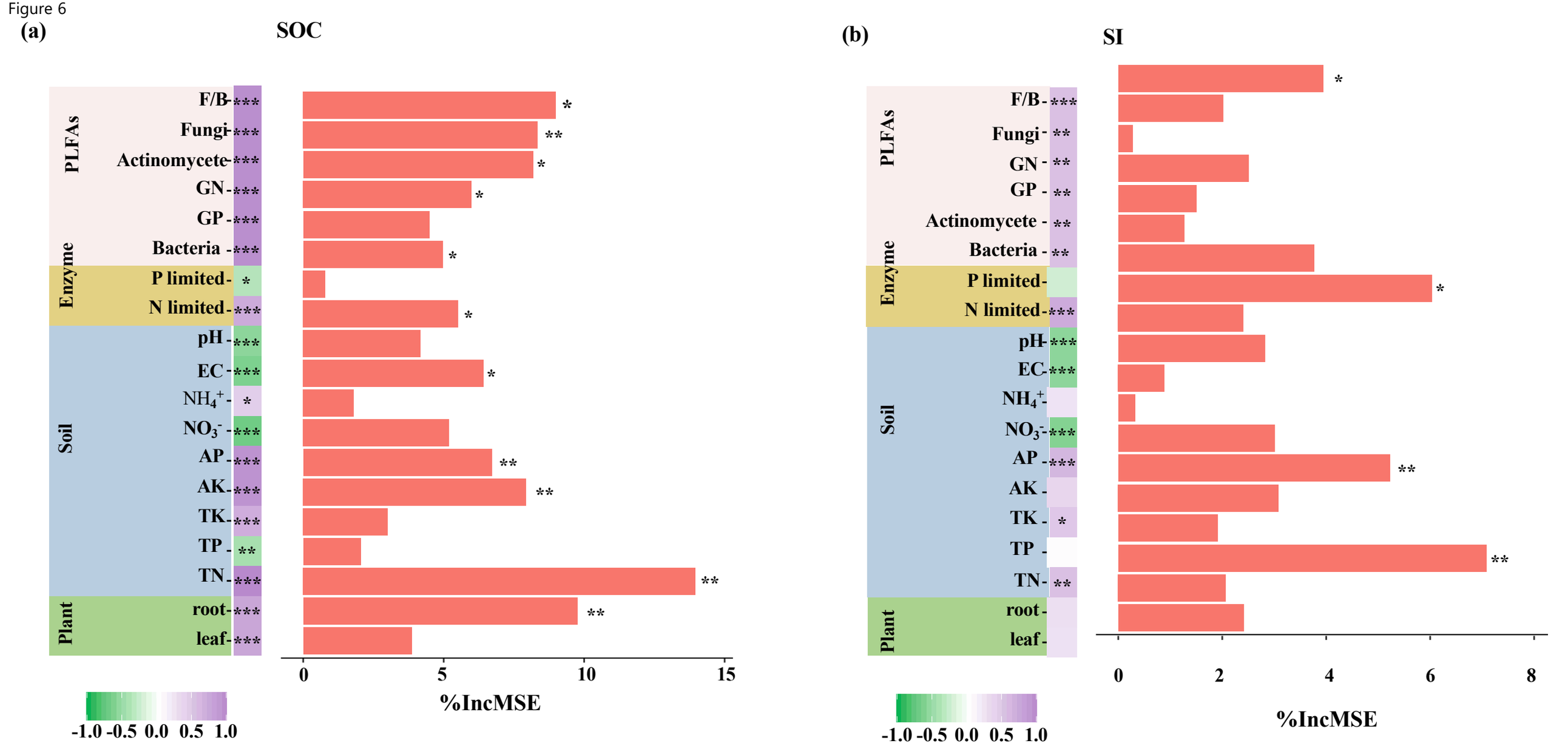
(a)
SOC
PLFAs
Enzyme
Soil
Plant
F/B
Fungi
Actinomycete
GN
GP
Bacteria
P limited
N limited
pH
EC
NH_4^+
NO_3^-
AP
AK
TK
TP
TN
root
leaf
0
5
10
15
%IncMSE
-1.0 -0.5 0.0 0.5 1.0
(b)
SI
0
2
4
6
8
%IncMSE
-1.0 -0.5 0.0 0.5 1.0

Figure 7

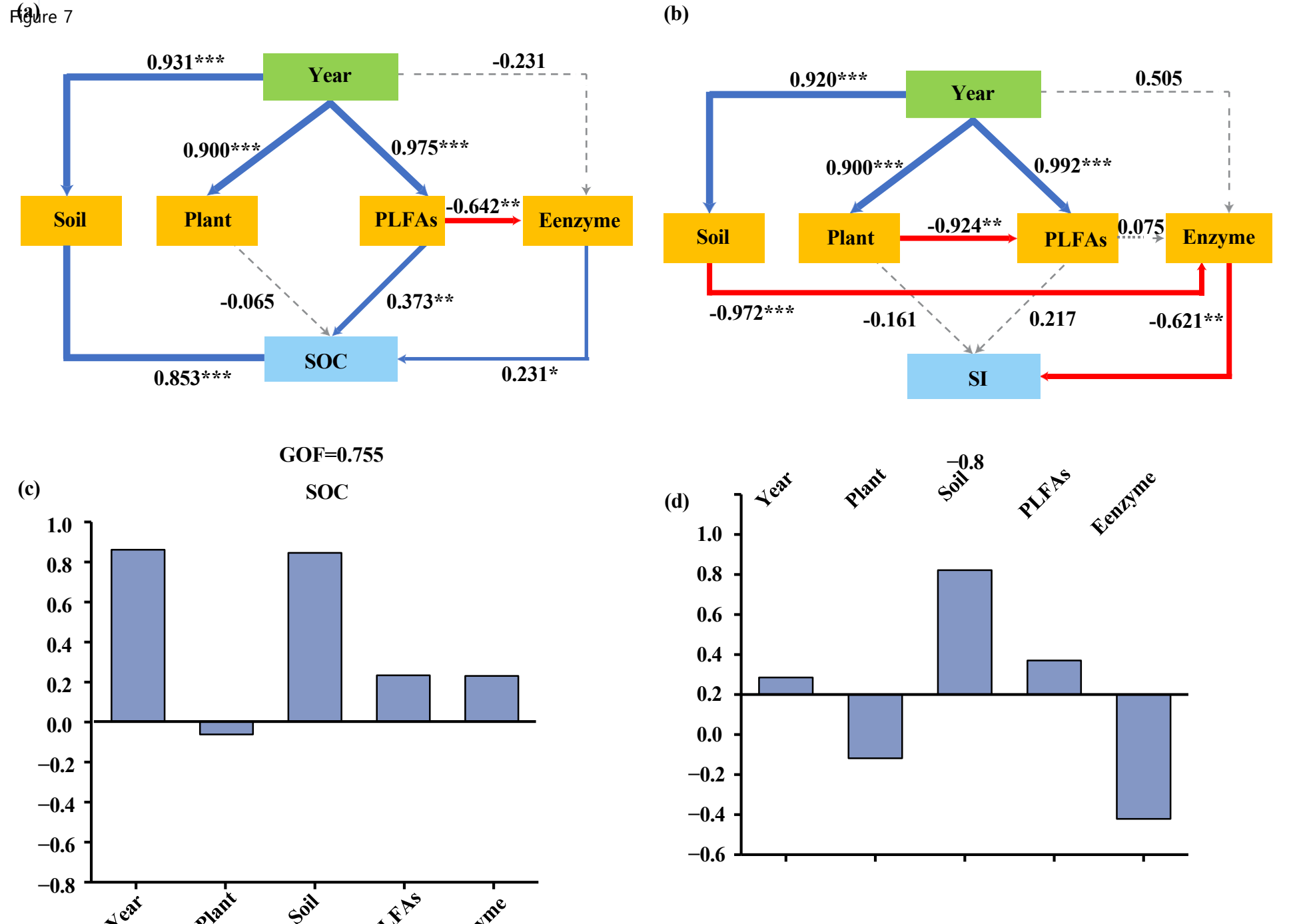
(a)
Year
Soil
Plant
PLFAs
Eenzyme
SOC
0.931***
-0.231
0.900***
0.975***
-0.642**
-0.065
0.373**
0.853***
0.231*
(b)
Year
Soil
Plant
PLFAs
Enzyme
SI
0.920***
0.505
0.900***
0.992***
-0.924**
0.075
-0.972***
-0.161
0.217
-0.621**
(c)
GOF=0.755
SOC
1.0
0.8
0.6
0.4
0.2
0.0
−0.2
−0.4
−0.6
−0.8
Year
Plant
Soil
(d)
Year
Plant
Soil
PLFAs
Eenzyme
1.0
0.8
0.6
0.4
0.2
0.0
−0.2
−0.4
−0.6

G

O

F

=

0

.

6

6

9

S

I

Figure S1

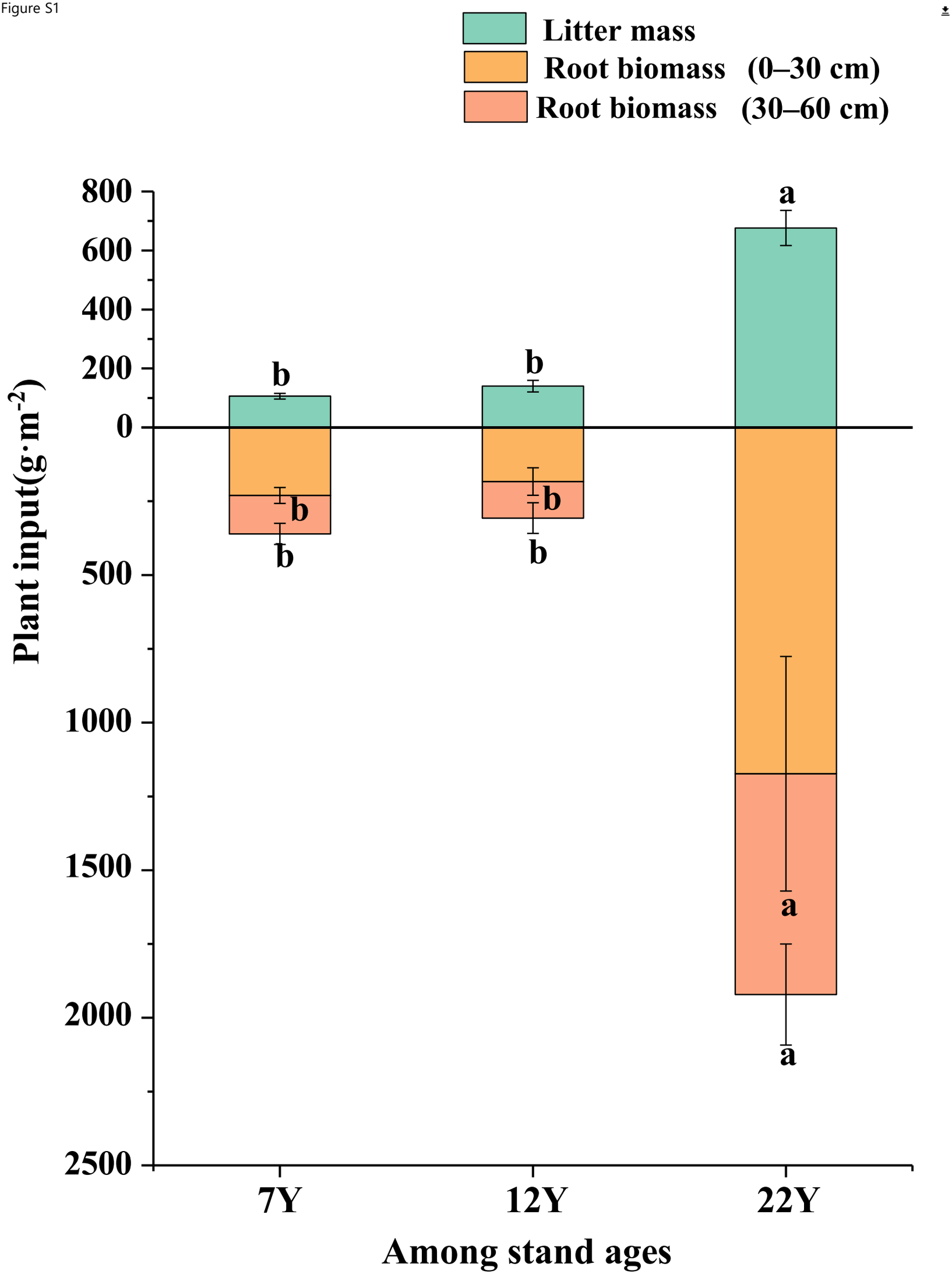
Litter mass
Root biomass (0–30 cm)
Root biomass (30–60 cm)
Plant input(g·m-2)
800
600
400
200
0
500
1000
1500
2000
2500
b
b
b
b
b
b
a
a
a
7Y
12Y
22Y
Among stand ages

Figure S2

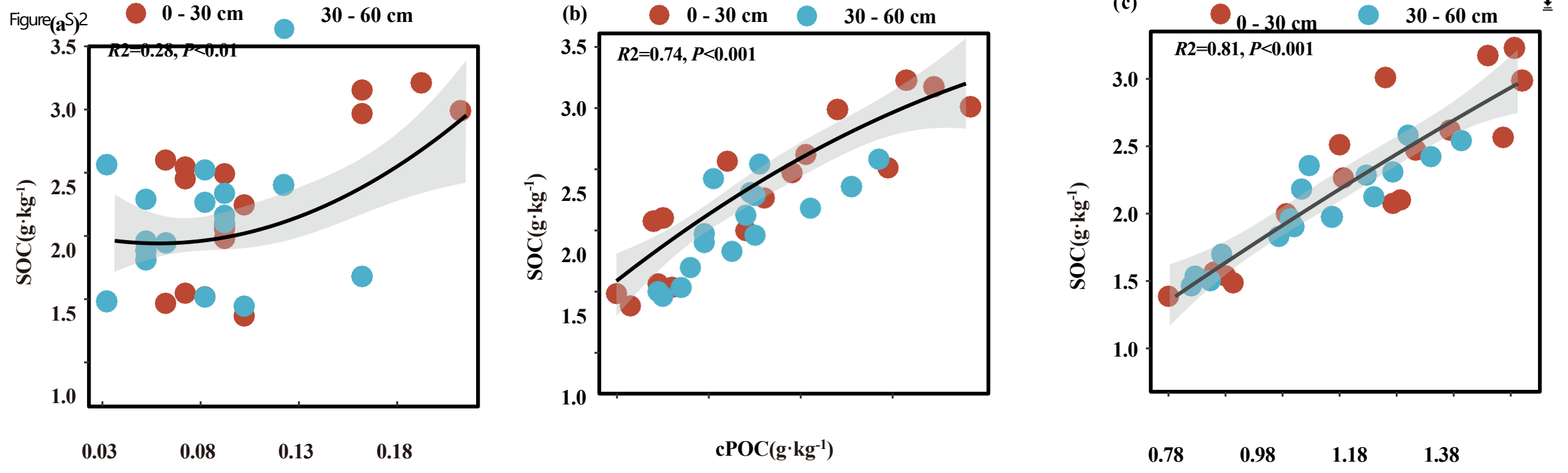
(a)
0 - 30 cm
30 - 60 cm
R2=0.28, P<0.01
SOC(g·kg-1)
3.5
3.0
2.5
2.0
1.5
1.0
0.03
0.08
0.13
0.18
(b)
0 - 30 cm
30 - 60 cm
R2=0.74, P<0.001
SOC(g·kg-1)
cPOC(g·kg-1)
(c)
0 - 30 cm
30 - 60 cm
R2=0.81, P<0.001
SOC(g·kg-1)
0.78
0.98
1.18
1.38

fPOC($g \cdot kg^{-1}$)

0.33 0.48 0.63 0.78 0.93 1.08 1.23

MAOC($g \cdot kg^{-1}$)

Figure S3

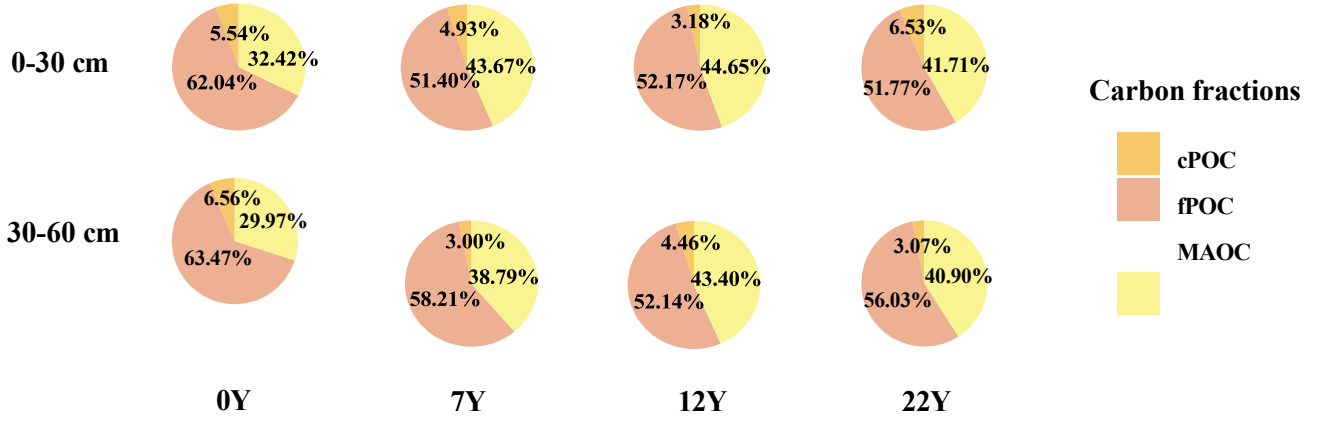
0-30 cm
30-60 cm
5.54%
32.42%
62.04%
4.93%
43.67%
51.40%
3.18%
44.65%
52.17%
6.53%
41.71%
51.77%
6.56%
29.97%
63.47%
3.00%
38.79%
58.21%
4.46%
43.40%
52.14%
3.07%
40.90%
56.03%
0Y
7Y
12Y
22Y
Carbon fractions
cPOC
fPOC
MAOC

Among stand ages

Figure S4

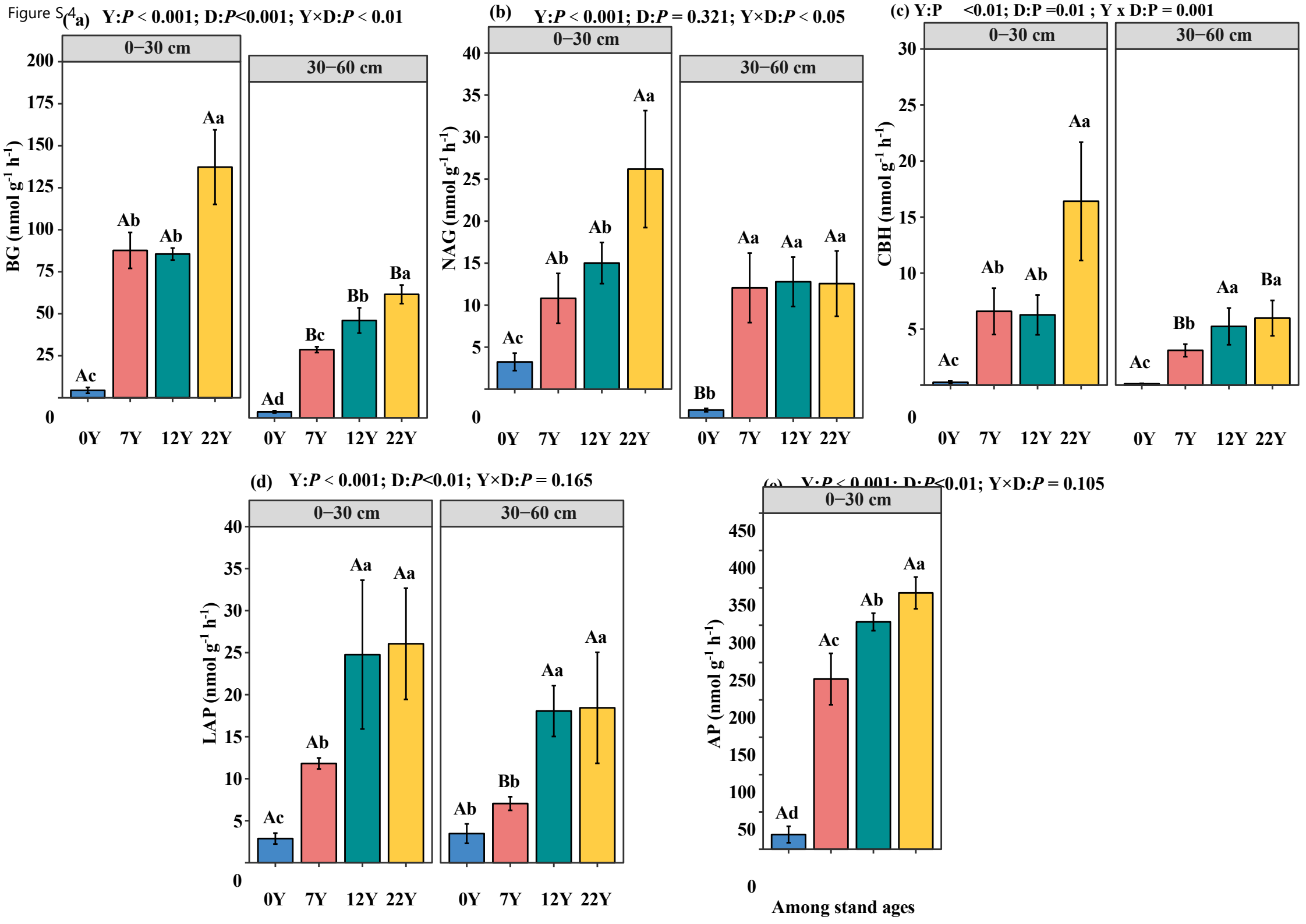
(a) Y:P < 0.001; D:P<0.001; Y×D:P < 0.01
(b) Y:P < 0.001; D:P = 0.321; Y×D:P < 0.05
(c) Y:P <0.01; D:P =0.01 ; Y x D:P = 0.001
(d) Y:P < 0.001; D:P<0.01; Y×D:P = 0.165
(e) Y:P < 0.001; D:P<0.01; Y×D:P = 0.105
0–30 cm
30–60 cm
BG (nmol g-1 h-1)
NAG (nmol g-1 h-1)
CBH (nmol g-1 h-1)
LAP (nmol g-1 h-1)
AP (nmol g-1 h-1)
0Y
7Y
12Y
22Y
Among stand ages

0Y 7Y 12Y 22Y 0Y 7Y 12Y 22Y

Figure S5

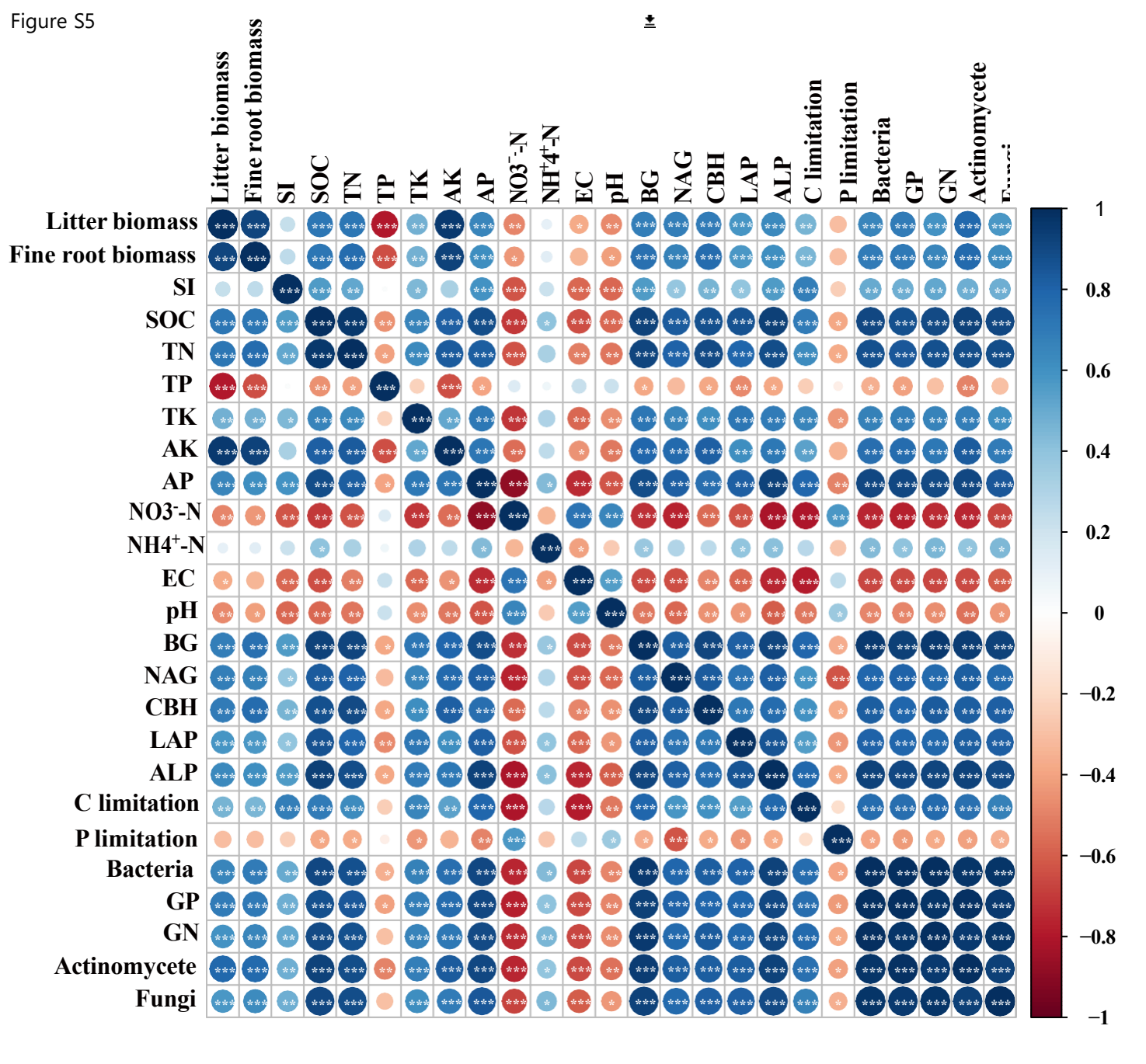
Litter biomass
Fine root biomass
SI
SOC
TN
TP
TK
AK
AP
NO3-N
NH4+-N
EC
pH
BG
NAG
CBH
LAP
ALP
C limitation
P limitation
Bacteria
GP
GN
Actinomycete
Fungi
1
0.8
0.6
0.4
0.2
0
−0.2
−0.4
−0.6
−0.8
−1

Figure S

Click here to access/download;Figure;Figure S6.pdf

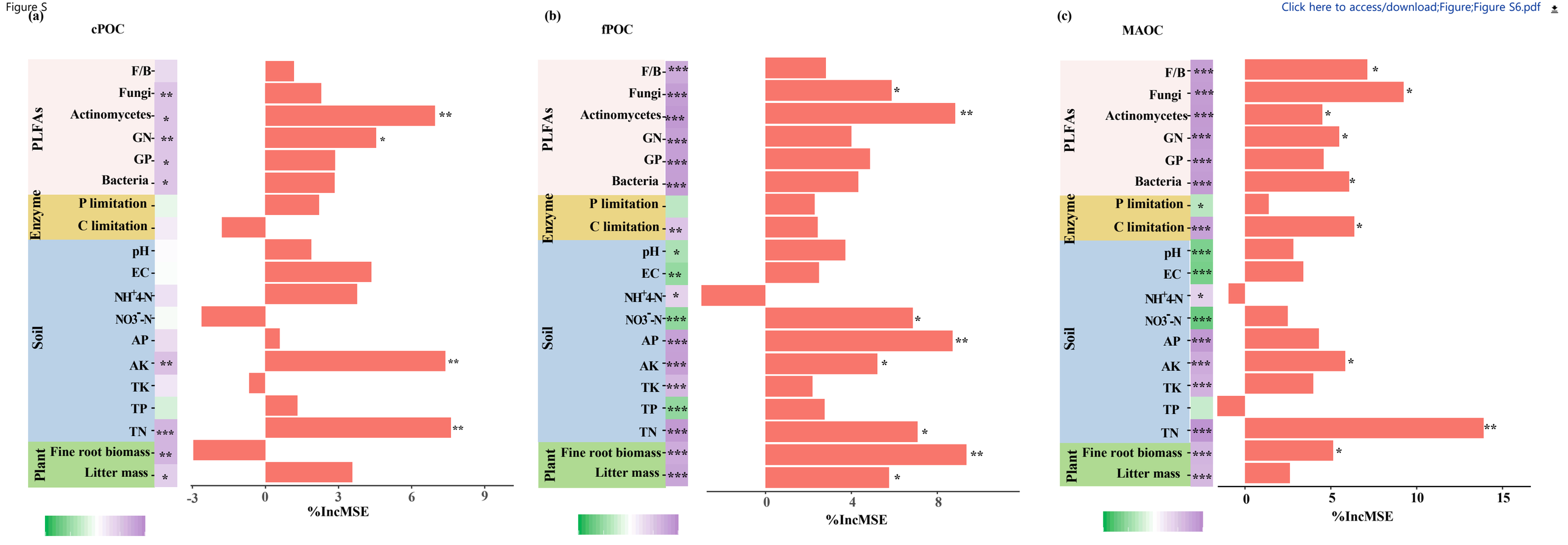

-1.0 -0.5 0.0 0.5 1.0

-1.0 -0.5 0.0 0.5 1.0

-1.0 -0.5 0.0 0.5 1.0

S